AN APPLICATION OF WAKE SURVEY RAKES TO THE EXPERIMENTAL DETERMINATION OF THRUST FOR A PROPELLER DRIVEN AIRCRAFT

NASA-CR-163920
19810007471

eirs
ENGINEERING & INDUSTRIAL RESEARCH STATION
AEROSPACE ENGINEERING

FINAL REPORT

by

K. R. Hall
S. J. Miley
H. J. Tsai

Mississippi State University
Mississippi State, MS 39762

MSSU-EIRS-ASE-81-3

SECURITY CLASSIFICATION OF THIS PAGE *(When Data Entered)*

REPORT DOCUMENTATION PAGE		READ INSTRUCTIONS BEFORE COMPLETING FORM
1. REPORT NUMBER MSSU-EIRS-ASE-81-3	2. GOVT ACCESSION NO.	3. RECIPIENT'S CATALOG NUMBER
4. TITLE *(and Subtitle)* An Application of Wake Survey Rakes to the Experimental Determination of Thrust for a Propeller Driven Aircraft		5. TYPE OF REPORT & PERIOD COVERED Final 6. PERFORMING ORG. REPORT NUMBER MSSU-EIRS-ASE-81-3
7. AUTHOR(s) Department of Aerospace Engineering Mississippi State University Drawer A Mississippi State, MS 39762		8. CONTRACT OR GRANT NUMBER(s) NSG-1454
9. PERFORMING ORGANIZATION NAME AND ADDRESS NASA Langley Research Center		10. PROGRAM ELEMENT, PROJECT, TASK AREA & WORK UNIT NUMBERS
11. CONTROLLING OFFICE NAME AND ADDRESS		12. REPORT DATE February, 1981 13. NUMBER OF PAGES 75
14. MONITORING AGENCY NAME & ADDRESS*(if different from Controlling Office)*		15. SECURITY CLASS. *(of this report)* Unclassified 15a. DECLASSIFICATION/DOWNGRADING SCHEDULE
16. DISTRIBUTION STATEMENT *(of this Report)*		
17. DISTRIBUTION STATEMENT *(of the abstract entered in Block 20, if different from Report)*		
18. SUPPLEMENTARY NOTES		
19. KEY WORDS *(Continue on reverse side if necessary and identify by block number)* Propeller, thrust, efficiency, wake survey, flight test		

20. ABSTRACT *(Continue on reverse side if necessary and identify by block number)*

The use of wake survey rakes for the in-flight determination of the resultant thrust for a constant-pitch propeller-driven, low-wing, single-engine general aviation aircraft was investigated. The lack of slipstream static pressure distribution seriously affected the results of this study but recommendations for removing the deficiency are discussed. The wake survey rake is shown to be a valuable tool in aircraft flight testing.

DD FORM 1 JAN 73 1473 EDITION OF 1 NOV 65 IS OBSOLETE

SECURITY CLASSIFICATION OF THIS PAGE *(When Data Entered)*

An Application of Wake Survey Rakes to the Experimental Determination of Thrust for a Propeller Driven Aircraft

by

K. R. Hall
S. J. Miley
H. J. Tsai

Report Number MSSU-EIRS-ASE-81-3

Prepared by

Mississippi State University
Engineering and Indsutrial Research Station
Department of Aerospace Engineering
Mississippi State, MS 39762

Final Report

Under NASA Grant No. NSG 1454

February 1981

LIST OF FIGURES

LIST OF SYMBOLS

C_p	coefficient of power
C_P	coefficient of pressure
C_t	coefficient of thrust
D	drag, aircraft alone
ΔD	incremental drag due to propeller slip stream
J	advance ratio, V/nD
K_ϕ	angle factor
K_p	pressure factor
K_v	velocity factor
K_{ps}	static pressure factor
P	static pressure
P_T	total pressure
ΔP	difference of pressure
Q	dynamic pressure
F	resultant horizontal force of aircraft
R_1	propeller radius to tip
r	radius distance from thrust axis to survey point
T	thrust
T_c	thrust coefficient
V	velocity
V_x	velocity component on X-axis
V_y	velocity component on Y-axis

V_z velocity component on Z-axis

α pitch angle

β yaw angle

γ ratio of specific heat of air at constant pressure to specific heat of air at constant volume

δ dihedral angle

η propeller efficiency

θ_n angle between the velocity vector and the nth pressure hole

ϕ conical angle

ρ air mass density

Subscripts:

0 station 0, plane ahead of propeller (free stream)

1 station 1, survey plane behind propeller

2 station 2, plane behind propeller where $P_2 = P_0$

SECTION 1

Introduction

The determination of drag on a propeller-driven aircraft in flight has always posed a problem for engineers. Since no direct means of measuring the total drag on an aircraft in flight exists at the present time, the drag is usually estimated from related flight test variables such as the thrust produced by the propulsive system. However, use of the thrust requires a knowledge of the propulsive efficiency of the aircraft for various flight conditions and engine operating conditions. Estimates of propulsive efficiency based upon empirical results or comparative performance testing can often produce uncertainties in the resulting data which may be unacceptable.

The manufacturers of general aviation aircraft currently employ a calibrated engine performance chart or measurements from an engine shaft thrust-torque transducer to determine the engine output. This value is then combined with a propeller efficiency value to determine the actual thrust. Problems arise in the use of this method as the propeller efficiency is determined using methods developed thirty years ago for isolated propellers of a different category. Optimization of aircraft performance through drag reduction based upon flight test programs is often considered unnecessary or unjustified unless performance falls far below expected levels. Drag effects cannot be separated from propulsion system effects, so no opportunity is available to inprove the design methods.

One method of directly determining engine-propeller thrust is by the use of wake survey rakes. This method has generated considerable

analytical interest (Ref. 1) and experimental interest (Ref. 5,6) due to the elegant simplicity of the apparatus. Experimental programs, wind tunnel tests, and flight tests employing wake survey rakes are reported in aviation literature from 1915 to 1950 (Ref. 5,7). This research includes isolated propellers, propellers in the presence of afterbodies, and high performance propeller driven aircraft (Ref. 7). The wake survey rake is potentially an excellent tool for flight testing by the general aviation industry. The instrumentation requirements are unsophisticated and consist of standard inventory items for most flight test activities. The data analysis can easily be accomodated by minicomputers.

This report is concerned with the investigation of the use of wake survey rakes in the determination of thrust, thrust distribution, and propulsive efficiency of a general aviation propeller driven aircraft. In addition, some of the flow characteristics in the wake of the propeller will be examined. The aircraft chosen for the test program is the Gulfstream American Yankee AA-1 aircraft, a low-wing single engine trainer. The experimental program is to instrument a full scale powered test program in the NASA 30 feet by 60 feet full-scale wind tunnel located at Langley Research Center. The entire test plan is detailed in Figure 4 of this report.

For the test program, an array of wake survey rakes was designed and fabricated. The rake configuration is detailed in Figures 1, 2, and 3 of this report. Each rake is composed of venturi type kiel tubes and five-hole directional pitot-static tubes as illustrated in Figure 2. Each test configuration utilizes four rakes mounted in an "X" arrangement as shown in Figure 3. To obtain more wake data, each test is rerun with

the rake configuration rotated one-eighth rotation about the propeller axis to provide a total of eight radial distributions of pressure measurements for accurate determination of flow characteristics in the wake. As shown in Figure 3, a second test configuration is chosen with the rakes moved to a position further aft of the propeller and the test is repeated for the new rake location.

The momentum theory of fluid dynamics will be applied to the determination of the propeller thrust from the pressure measurements available from the wake survey rakes. The theory used in the thrust determination will be reviewed and the measurement results will be compared to the data from the tunnel external balance system and to the data from the propeller thrust-torque rotary balance. The flow directions in the propeller wake will be investigated by use of the five-hole pitot-static pressure measurements.

One might note that the use of propeller thrust force transducers for measuring propeller shaft thrust was employed by the Curtis-Wright Corporation (Ref. 10,11). This work confirmed the earlier work (Ref. 12) that the shaft thrust is amplified by blockage effects of the afterbody. Propeller efficiencies exceeding 100% can be obtained for blunt afterbodies of sufficient cross-sectional area. Referring to Reference 13 and to Figures 28 and 31 of this report, one may gain some appreciation for this shortcoming.

SECTION 2.1

Theory

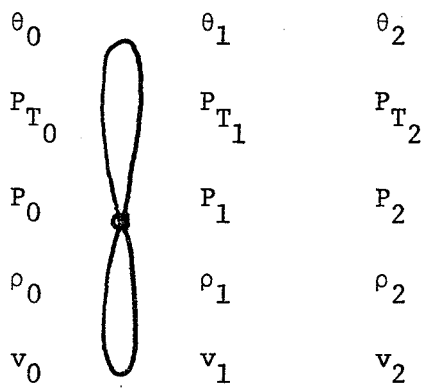

Figure 2.0 Stations employed in Linear Momentum theory.

From Figure 2.0, let the quantities with a zero subscript be measured in front of the propeller plane; let the quantities with a one subscript be measured just aft of the propeller plane; and let quantities with a two subscript be measured aft of the propeller where $P_2 = P_0$. The effect of the propeller on the air passing through its disc will be to cause an increase in the static pressure without causing an increase in velocity or a change in density. This is the classical "actuator disc" theory.

Between stations zero and two, the thrust produced by the propeller causes a change in the linear momentum of the air passing into a control volume at station zero and out of the control volume at station two. Applying the theory of linear momentum and considering continuity of mass between stations zero and one and two yields the following differential equation for the thrust.

$$\frac{dT}{dA_1} = \rho_1 v_1 (v_2 - v_0)$$

The velocity terms appearing in the equation above may be expressed in terms of pressures and densities by using the following relationship from compressible aerodynamics (Ref. 2).

$$\frac{P_T}{P} = \left[1 + \frac{\gamma - 1}{2} M^2\right]^{\frac{\gamma}{\gamma - 1}} = \left[1 + \frac{\gamma - 1}{2\gamma} \frac{\rho v^2}{P}\right]^{\frac{\gamma}{\gamma - 1}}$$

Solving for velocity from the expression above yields:

$$v_k^2 = \left(\frac{2\gamma}{\gamma - 1}\right)\left(\frac{P_k}{\rho_k}\right)\left[\left(\frac{P_{T_k}}{P_k}\right)^{\frac{\gamma - 1}{\gamma}} - 1\right]$$

Use $\gamma = 1.4$ for air and replace the velocities in the differential equation for thrust to obtain

$$\frac{dT}{dA_1} = 7P_1 \left[R_1 - 1\right]^{1/2} \left[R_2^{1/2}(R_3 - 1)^{1/2} - R_4^{1/2}(R_5 - 1)^{1/2}\right]$$

where $$R_1 = \left(\frac{P_{T_1}}{P_1}\right)^{2/7}$$

$$R_2 = \frac{P_2}{\rho_2}\frac{\rho_1}{P_1}$$

$$R_3 = \left(\frac{P_{T_2}}{P_2}\right)^{2/7}$$

$$R_4 = \frac{P_0}{\rho_0}\frac{\rho_1}{P_1}$$

$$R_4 = \left(\frac{P_{T_0}}{P_0}\right)^{2/7}$$

Assume isentropic flow $\left(\frac{P}{\rho^\gamma} = \text{Constant}\right)$ everywhere except through the propeller disc and assume constant density of the air passing through

the propeller disc to obtain

$$\frac{dT}{dA_1} = 7P_1^{5/7} (D_1)^{1/2} [(D_1)^{1/2} - (D_0)^{1/2}]$$

where $D_0 = P_{T_0}^{2/7} - P_0^{2/7}$

$$D_1 = P_{T_1}^{2/7} - P_1^{2/7}$$

Lastly, assume $P_1 = P_0 + \Delta P$ and $P_{T_1} = P_{T_0} + \Delta P$ where ΔP is a small quantity. The differential equation may then be expanded in a series concerning ΔP.

Neglecting terms of order $O(\Delta p^2)$ and above yields the following expression for the differential thrust.

$$\frac{dT}{dA_1} = \left[\frac{P_0}{P_{T_0}}\right]^{5/7} \Delta P$$

This last expression allows the determination of the differential thrust from measurement of the free stream conditions and the pressure differential across the propeller plane. By integrating over the propeller disc area, the total thrust can be obtained.

$$dA_1 = d(\pi r^2) = \pi R_1 \, d\left(\frac{r}{R_1}\right)^2$$

The differential area is now a function of the propeller outer radius R_1 and the non-dimensional variable $\frac{r}{R_1}$.

Define the quantity to be measured to be a pressure coefficienty given by the following equation

$$C_P = \frac{P_T - P_0}{q_0}$$

where P_0 and q_0 are free stream static and dynamic pressures, respectively.

Since $\Delta P = P_T - P_{T_0}$,

$$\Delta P = (P_T - P_0) - (P_{T_0} - P_0) = C_p q_0 - q_0 = (C_p - 1) q_0$$

Now, $\frac{dT}{dA_1} = \frac{dT}{\pi R_1^2 d(\frac{r}{R_1^2})} = [\frac{P_0}{P_{T_0}}]^{5/7}(C_p-1)q_0$

Define $T_c = \frac{T}{\pi R_1^2 q_0}$ as the thrust coefficient, which should not be confused with $C_T = \frac{T}{\rho N^2 D^4}$, the coefficient of thrust.

Now, the differential equation for thrust can be written in non-dimensional form as follows

$$\frac{d\ (T_c)}{d\ (\frac{r}{R_1})^2} = [\frac{P_0}{P_{T_0}}]^{5/7}\ (C_p-1)$$

This expression is used in generating Figures 8 through 24 which show the thrust coefficient distribution for various tunnel operating speeds and for various propeller operating speeds and for various rake locations for pressure coefficient measurements.

Since only a finite number of pressure coefficients can be measured along one radial line and only a finite number of radial lines can be employed, a method of data fitting and approximation was employed. For a given number of pressure coefficients measured in one radial direction, a cubic spline approximation to the continuous pressure coefficient distribution is calculated and this spline approximation is then integrated to give a thrust coefficient. Other radial distributions are treated in a similar manner to yield several thrust coefficients which are averaged to yield a single thrust coefficient for the given operating condition. This thrust coefficient may then be multiplied by q_0 and the propeller disc area to obtain the thrust force for the given operating

condition. A summary of the integrations is presented in Figures 25 and 26.

The thrust and power of a propeller are usually expressed in coefficient form and the ones which are generally used are the coefficient of thrust (C_T) and the coefficient of power (C_P). These two coefficients are defined by

$$C_T = \frac{T}{\rho N^2 D^4}$$

$$C_P = \frac{P}{\rho N^3 D^4}$$

where ρ is density, N is the propeller speed in revolutions per second, and D is the propeller diameter in the appropriate units. Note that ND corresponds to a velocity and D^2 corresponds to an area. An additional nondimensional variable is obtained from this observation. Define the nondimensional velocity coefficient J, called the advance ratio, by the following expression

$$J = \frac{V}{ND}$$

Lastly, the propeller efficiency η is defined to be the ratio of the output power to the input power. The following equation shows the definition in terms of the dimensional thrust, velocity, and power and also in terms of the nondimensional coefficient of thrust, advance ratio, and coefficient of power.

$$\eta = \frac{TV}{P} = \frac{C_T J}{C_P}$$

As stated in Reference 9, "one would expect these dimensionless coefficients

to be a function only of the flow geometry (excluding scale effects such as Mach number and Reynolds number)."

These coefficients are calculated and presented for the two different rake locations and for representative tunnel operating conditions and propeller operating conditions in Figures 27-32.

Section 2.2

USE OF 5-HOLE PITOMETER TO CALCULATE FLOW ANGLE AND STATIC PRESSURE

A 5-hole pitometer (Fig.2.1) is used for the measurement of direction and velocity of air stream. The relation between the flow parameters and the pressure distribution over the probe was basically obtained from potential flow theory [Ref. 2]. The notation for the spherical sensing head is shown in figure 2.1.

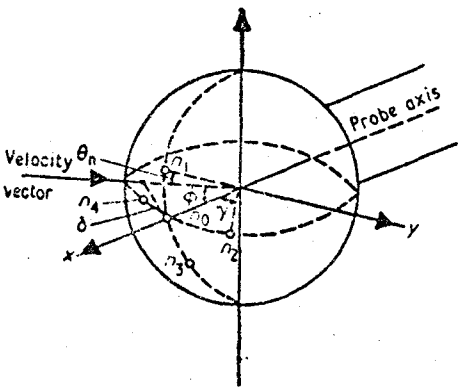

Figure 2.1

Where:

ϕ: Conical angle formed by the velocity vector and probe axis.

δ: Dihedral angle between the flow plane and the meridian plane.

θ_n: Angle between the velocity vector and the nth pressure hole.

By selecting appropriate reference axes the angle θ_n can be expressed in terms of easily measured angles using spherical trigonometric relations. Two commonly used pairs of angles in which θ_n is expressed are (i) the pitch α and yaw β angles (shown in Figure 2.1)

and (ii) the conical angle ϕ and dihedral angles δ (shown in Figure 2.1).

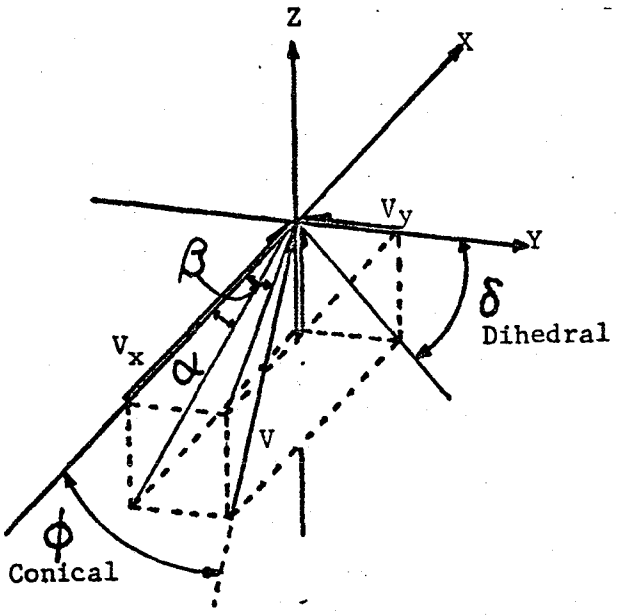

Figure 2.2

The probes were calibrated according to the method evaluated by M. A. Wright [Ref. 8]. The prime calibration function is angle factor K_ϕ;

$$K_\phi = \{1 - \sum_{n=1}^{4}(Pe_o - Pe_n)/2[\sum_{n=1}^{4}(Pe_o - Pe_n)^2]^{1/2}\}^{1/2}$$

Pe_n: is the static pressure at point n on the surface (Figure 2.2).

This function uses the five probe pressures (i.e., Pe_n, n = 0,4) and is the independent calibration variable. Dependent calibration variables are as follows: Velocity factor K_v,

$$K_v = \{\rho V^2[\sum_{n=1}^{4}(Pe_o - Pe_n)^2]^{-1/2}\}^{1/2}$$

Pressure factor K_p,

$$K_p = 2(Pe_o - P_s)/\rho V^2$$

where

P_s is free stream static pressure.

The conical flow angle ϕ is related to K_ϕ by polynomial curve fit, [Ref. 8].

$$\phi = 0.8509K_\phi + 0.3008K_\phi^3 - 0.0879K_\phi^5 \quad \text{(in radian)}$$

Wright showed that with a small magnitude of error both K_v and K_p can be expressed as a function of ϕ only. This expression can be used satisfactorily for most applications over the range of ϕ covered. The functions for K_v and K_p are shown below:

$$K_v = 1.0297 + 0.0705\phi^2 + 0.0266\phi^4$$

$$K_p = 4.5 \exp(-0.3946\phi^2) - 3.5$$

The dihedral angle δ used here is modified from Wright and is defined as: [Ref. 4]

$$\delta \equiv [(Pe_2 - Pe_4)/(Pe_1 - Pe_3)]$$

Both yaw angle β and pitch angle α can be calculated from the three components of the free stream velocity, by using trigonometric relations. From Figure 2.2, the relationship among these three velocity components

V_x, V_y, V_z, and α, β is shown

$$\alpha = \tan^{-1}\left(\frac{V_z}{V_x}\right) \tag{1}$$

$$\beta = \tan^{-1}\left(\frac{V_y}{V_x}\right) \tag{2}$$

Also from Fig. 2.1

$$V_x = V \cos \phi \tag{3}$$

$$V_y = V \sin \phi \cos \delta \tag{4}$$

$$V_z = V \sin \phi \sin \delta \tag{5}$$

By substituting equation (3), (4), (5) into equation (1), (2), they become:

$$\alpha = \tan^{-1}(\tan \phi \sin \delta)$$

$$\beta = \tan^{-1}(\tan \phi \cos \delta)$$

A numerical example is presented in the following section.

NUMERICAL EXAMPLE FOR 5-HOLE PITOMETER

Flow directions, velocity, and static pressure can be calculated by following procedures listed below:

A group of measured pressure data is:

$$Pe_o = 1.1805 \times 10^5 \qquad Pe_3 = 1.0282 \times 10^5$$

$$Pe_1 = 1.0204 \times 10^5 \qquad Pe_4 = 1.0451 \times 10^5$$

$$Pe_2 = 1.0173 \times 10^5 \qquad \text{(in } N/M^2\text{)}$$

1) Substituting pressure differentials into the K_ϕ equation

$$K_\phi = \{1 - \sum_{n=1}^{4}(Pe_o - Pe_n)/2[\sum_{n=1}^{4}(Pe_o - Pe_n)^2]^{1/2}\}^{1/2}$$

$$K_\phi = 0.0497$$

2) Substituting $K_\phi = 0.04976$ into the ϕ equation gives

$$\phi = 0.04237 \text{ rad.} \quad (2.432°)$$

3) Substituting pressure differentials $(Pe_2 - Pe_4)$, $(Pe_1 - Pe_3)$ into the δ equation gives dihedral angle

$$\delta = 74.24°$$

4) Substituting δ and ϕ into the α and β equations gives

$$\alpha = 2.341°$$

$$\beta = 0.661°$$

5) Substituting the calculated value of ϕ into the K_v equation gives

$$K_v = 1.0298$$

6) Substituting $K_v = 1.0298$ into the V equation gives velocity.

Taking $\rho = 1.2$ Kg/M^3;

$$V = \{K_v^2[\sum_{n=1}^{4}(Pe_o - Pe_n)^2]^{1/2}/\rho\}^{1/2}$$

$$V = 13.9141 \quad M/Sec$$

7) The static pressure is calculated by determining the value of K_p from the K_p equation for the calculated value of $\phi = 0.04237$

$$K_p = 4.5 \cdot EXP(-0.3946\phi^2) - 3.5$$

$$K_p = 0.9968$$

The values of K_p and K_v are used to calculate the static pressure function K_{ps} [Ref. 8].

$$K_{ps} \equiv K_p \cdot K_v^2$$

$$K_{ps} = 1.0571$$

From the equation defining K_{ps}

$$K_{ps} = \frac{2(Pe_o - P_s)}{[\sum_{n=1}^{4}(Pe_o - Pe_n)^2]^{1/2}}$$

Solve the above equation for P_s:

$$P_s = Pe_o - \frac{[\sum_{n=1}^{4}(Pe_o - Pe_n)^2]^{1/2}}{2} \cdot K_{ps}$$

$$P_s = 1.1805 \times 10^5 - 1.5316 \times 10^4 \cdot 1.0571$$

$$= 1.0186 \times 10^5 \quad (N/M^2)$$

Summary of results of example:

In-flow angle (α) = 2.341°

Swirl angle (β) = 0.661°

Velocity = 13.914 M/sec

Static pressure = 1.019×10^5 Newton/M^2

SECTION 2.3

Horizontal Force Resultant on a Propeller Powered Aircraft

The resultant horizontal force acting upon a propeller powered aircraft is composed of three components: the propeller thrust, the drag of the basic airframe without the propeller at the operating condition, and the additional component of drag due to the presence of the propeller and the attendent slipstream.

$$F = T - D - \Delta D$$

where F is the resulting horizontal force

T is the thrust of the propeller

D is the drag of the basic airframe

ΔD is the drag increase with propeller running.

The effective thrust of the propeller is the resultant horizontal force plus the drag of the basic airframe

$$F + D = \text{effective thrust} = T - \Delta D$$

This means that the total thrust force produced must be decreased by the amount of drag imparted to the aircraft by the propeller operation to produce the effective thrust of the propeller.

In a similar manner, the total drag acting upon a propeller powered aircraft is composed of two components: the drag of the basic airframe without the propeller, and the increment in drag due to the presence of the operating propeller and its slipstream.

$$D + \Delta D = \text{Total Drag}$$

From this discussion, one may see the difficulty of separating the thrust effects from the drag effects for a propeller powered aircraft.

SECTION 3.1

Experimental Apparatus

The full-sized test aircraft was chosen to be a Gulfstream American Yankee, a single engine, low-wing, trainer type of aircraft with non-retractable landing gear and powered by a Lycoming O-235-C2C engine with a constant pitch propeller. The size, performance, and flight characteristics of this aircraft are typical for modern single-engine general aviation type of aircraft.

The 30 feet by 60 feet full-scale wind tunnel at the NASA Langley Research Center was employed for the test. This tunnel allows the full-sized airplane to be tested as if in flight. The available instrumentation for the tunnel includes an external force balance, various pressure transducer measuring apparatus, and a propeller thrust/torque balance.

Wake survey rakes which utilized the pressure transducer equipment were fabricated to measure the total pressure distribution in the radial direction behind the propeller disc. The rakes, as described in Figures 1, 2, and 3, consist of an array of Kiel (K) total pressure probes and 5-hole hemispherical (S) pressure probes. The locations and dimensions for a typical rake are shown in Figure 1. These probes were mounted to a streamlined steel mount and an extension piece was added to the rake positioned on top of the cowl. At all times, the probe labeled S_2 was positioned at the propeller tip.

The 5-hole hemispherical probes were to measure total pressure, static pressure, and flow angularity as discussed earlier. The configuration for the individual probes are shown in Figure 2. The

identification of the holes on the 5-hole probe are as follows:

0 = Total pressure

1 = 12 o'clock pressure

2 = 3 o'clock pressure

3 = 6 o'clock pressure

4 = 9 o'clock pressure

It is extremely important that these rakes be mounted such that the 5-hole probe axis is parallel to the thrust axis or at some small known angle to the thrust axis.

There were four rakes fabricated for the test and there were four test configurations for the four rakes. Two of the test configurations provided eight radial pressure distributions for a given cowl position by running the same test twice, but rotating the rakes by 1/8 revolution about the cowl for the second test. Two cowl positions completed the test configurations as illustrated by Figure 3.

In addition to the wake rakes, static pressure measurements were available for the cowl in the form of an array of flush-mounted pressure ports from the spinner to the firewall. These were employed to obtain the influence of the cowl on the linear momentum of the slipstream.

SECTION 3.2

Analysis of Data

The process of data reduction and analysis is a systematic method of converting the test data into a standard format so that the information can be used to evaluate the result. The test data in this case consists of the tunnel operating conditions, the standard tunnel measurements of freestream conditions, the external force balance measurements, the thrust/torque balance measurements, and the pressure data available from the pressure transducers. A computer program was employed to take the data from magnetic tape and reproduce the data in a more useful form.

The pressure coefficients available from the wake rakes were converted into thrust coefficients by using the integration of the distribution

$$\text{Total } T_c = \int_0^{1.21} \left[\frac{P_0}{P_{T_0}}\right]^{5/7} (C_p - 1)\, d\left(\frac{r}{R_1}\right)^2$$

This corresponds to integrating 10% beyond the radius of the propeller disc. Four thrust coefficients were generated for each test configuration. The measurements from rake 1 were erratic and seem to indicate a partially blocked probe, so the results of rake 1 were deleted and the other three rakes were averaged to obtain a value of thrust and a corresponding coefficient of thrust. Once again, a cubic spline was used to obtain continuous pressure coefficient distributions from the discrete samples and also to integrate the resulting distribution.

The static pressure measurements made on the cowling were mapped into a 13 by 17 array. The cowl was then divided into 103 small, flat

panels where each panel contains four ports. The pressure distributions were considered linear between ports and a force on the panel determined. A mapping of the geometry of the cowling and the pressure ports allows the determination of the component of force on each panel in the direction of the thrust axis. This force acts upon the airplane, so an equal and opposite force is applied to the air in the slipstream by the cowling. This force should be taken into account in the linear momentum expression as it is an external force to the slipstream control volume.

SECTION 4

Results and Conclusions

The use of the 5-hole hemispherical head probes to measure the static pressure in the slipstream was not successful as the readings of the pressure data from the various probes were not consistent. The lack of slipstream static pressure data required that the approximate expression for thrust coefficient in terms of the measured freestream conditions and the measured pressure coefficients from the total pressure probes be employed. This approximation is a potential source of error and can be removed by adding static pressure measurements alongside each total pressure measurement. The 5-hole probes were used to determine the swirl angle and the inflow angle in the wake of the propeller. These data are presented in Figures 33-35 for representative descriptions.

The total pressure probes on the wake survey rake were the simplest and most reliable measurements made. Ideally, the runs considered in this report were made at zero sideslip and zero angle of attack. The use of more than one rake and the averaging of the thrust coefficients for one configuration provided a means of downplaying any misalignment of the aircraft or the rakes mounted upon the aircraft. Since aircraft in flight might use this method of thrust measurement, the recommended locations of the minimal rake configuration are at 3 o'clock and 9 o'clock. These locations are pictured on the aircraft shown in Figures 39-40. The lack of pressure measurements for the inner portion of the propeller disc provided another source of error as a smooth curve from the first radial pressure measurement was drawn to zero at the propeller thrust axis. A recommendation at this point is for more pressure measurements

made all along the radial line from propeller hub to tip or at least as many as feasible, consistent with experimentation and instrumentation requirements.

Figure 5 is the NACA gray chart relating coefficient of thrust and coefficient of power to the advance ratio for various propeller blade angles. This chart should be used as a comparison figure for most of the work presented in this report. Two different propellers are in popular use with the GA Yankee and Figures 5 and 7 present estimates of the propeller efficiency versus advance ratio for these two propellers. The solid line in Figure 7 represents the propeller used in this series of tests. Again, these values are presented for reference value only.

Figures 8, 9, and 10 represent measurements of the static thrust made using the aft position of the wake rakes for low, medium, and high propeller speeds. Figure 8 is made using a propeller RPM of 1200 and a tunnel RPM of 0. Tip vortex formation is apparent. Figure 9 is made using a propeller RPM of 1800 and a tunnel RPM of 0. The tip vortex formation is even more apparent. Figure 10 is made with a propeller RPM of 2200 and a tunnel RPM of 0. The vortex formation is most apparent and some rake misalignment may be suspected. The numerical values for the important quanitities associated with these figures are presented in Figures 25 and 26 as a summary of the data presented in Figures 8 through 24. The graphical presentations are intended to illustrate the flow characteristics for the individual rakes and to illustrate that the rakes do extend to the freestream conditions beyond the propeller tip.

Figures 11, 12 and 13 represent measurements of thrust made using the aft position of the wake rakes for low, medium and high propeller

speeds and a moderate tunnel speed. Figure 11 is made using a propeller RPM of 1200 and a tunnel RPM of 90. A discrepancy may be noted between Rake 4 and the other rakes which may be attributed to one or more blocked probes. Figure 12 is made using a propeller RPM of 1800 and a tunnel RPM of 90. The discrepancy between Rake 4 and the other rakes is even more apparent in this figure. Figure 13 is made using a propeller RPM of 2400 and a tunnel RPM of 90. Rake 4 still displays the discrepancy in this figure. The actual numerical values for these figures are presented in Figures 25 and 26.

Figures 14, 15, and 16 represent measurements of thrust made using the aft position of the wake rakes for low, medium, and high propeller speeds using a propeller RPM of 1200 and a tunnel RPM of 170. It is apparent from the figure that Rake 4 still displays discrepancy and that Rake 1 is not believable. Figure 15 is made using a propeller RPM of 1800 and a tunnel RPM of 170. Rake 4 still displays characteristic behavior for a rake with blocked probes and Rake 1, while still not in line with the other rakes, displays a more believable behavior. Figure 15 is made using a propeller RPM of 2400 and a tunnel RPM of 170. The outer portion of Rake 4 displays erratic behavior completely out of agreement with the other rakes. Again, the numerical results of these figures are summarized in Figures 25 and 26.

Figures 17, 18, and 19 represent measurements of static thrust made using the forward position of the wake rakes for low, medium, and high propeller speeds. Figure 17 is made using a propeller RPM of 1600 and a tunnel RPM of 0. The movement of the rakes to the forward position on the cowling seems to have corrected the aberrant behavior of Rake 4

while Rake 1 continues to display pressure distributions lower than the other rakes. Figure 18 is made using a propeller RPM of 1800 and a tunnel RPM of 0. Note that all rakes show agreement except near the propeller tips where vortices form. Figure 19 is made using a propeller RPM of 2400 and a tunnel RPM of 0. Note the agreement of Rakes 1 and 2 and the agreement of Rakes 3 and 4. This indicates misalignment of the aircraft or of the rakes mounted on the aircraft. Numerical results are summarized in Figures 25 and 26.

Figures 20, 21, and 22 represent measurements of thrust made using the forward position of the wake rakes for low, medium, and high propeller speeds. Figure 20 is made using a propeller RPM of 1200 and a tunnel RPM of 90. The wake rakes were rotated about the cowling by one-eighth revolution for these runs and the blocked probe syndrome has reappeared. Rake 1 displays the characteristics of blockage now and Rakes 2, 3, and 4 show fairly consistent readings. Figure 21 is made using a propeller RPM of 1800 and a tunnel RPM of 90. Again note the unreliable status of Rake 1 and the close agreement of the other rakes. Figure 22 is made using a propeller RPM of 2200 and a tunnel RPM of 90. Rake 1 is totally unreliable and the other rakes show close agreement. The numerical results of these figures are summarized in Figures 25 and 26.

Figures 23 and 24 represent measurements of thrust made using the forward position of the wake rakes for medium and high propeller speeds. Figure 23 is made using a propeller RPM of 1800 and a tunnel RPM of 170. Note that Rake 1 is unbelievable and the other rakes show close agreement. Figure 24 is made using a propeller RPM of 2200 and a tunnel RPM of 170. Rake 1 is unusable and the other rakes agree. The numerical results appear in Figures 25 and 26.

Figure 25 is a summary of the numerical results of Figures 8 through 24 in gravitational units of lb/ft/sec and Figure 26 is a summary of these same results in SI units of N/M/sec. The definitions of the column headings are as follows:

run: identification for tunnel test (given on figures)

QBR: tunnel free stream dynamic pressure

VEL: tunnel free stream speed

RPM: propeller revolutions per minute

TRQ: torque from thrust/torque meter

THB: thrust from thrust/torque meter

ETA: propeller efficiency from thrust/torque meter

J: advance ratio

CT: coefficient of thrust from thrust/torque meter

CP: coefficient of power from thrust/torque meter

THR: thrust from wake rake measurements

CTR: coefficient of thrust from wake rake

ETAR: propeller efficiency from wake rake

Figure 27 is a conventional diagram of coefficient of thrust versus advance ratio for the values taken from the thrust/torque meter and for the values taken from the wake rake in the forward position (with Rake 1 discarded). It is believed that the values from the thrust/torque meter are too large due to blockage effects mentioned earlier. It is also believed that the wake rake values are too low due to the absence of static pressure measurements in the propeller slipstream and the attendant approximation used. Ths true values of C_t therefore should lie between the values from the wake rake and the values from the thrust/

torque meter. Figure 28 is a diagram of propeller efficiency versus advance ratio for the same data and the same conclusions apply. The true values should lie between values taken from the wake rake and values taken from the thrust/torque meter. Figure 29 is a cross-plot of coefficient of thrust versus propeller efficiency for the same data and the conclusions previously stated still apply.

Figure 30 is a conventional diagram of coefficient of thrust versus advance ratio for the values taken from the thrust/torque meter and for the values taken from the wake rake in the aft position. Again, these values are presumed to be boundaries for the true values. Figure 31 is a diagram of propeller efficiency versus advance ratio for the aft rake position. Note that the thrust/torque meter is suggesting propeller efficiencies in excess of 100% which is not believable while the wake rake efficiencies still remain in the believable range. These values again should be taken as upper and lower boundaries on the true values. Figure 32 is a cross-plot of coefficient of thrust versus propeller efficiency for this same data and the same conclusions apply.

Figures 33, 34 and 35 represent values of the swirl angle and the inflow angle for various propeller speeds and tunnel speeds as calculated from the data from the 5-hole probes. They show the curvature of the slipstream as it is affected by the propeller for the forward rake position in Figure 33 and for the aft rake position in Figures 34 and 35.

The photograph of Figure 36 shows the GA-Yankee mounted in the full size tunnel at NASA Langley Research Center for this test, and Figure 37 shows an alternate view of the same test. Figure 38 shows the cowling of the Yankee dismounted and taped to distinguish the static pressure taps on the cowling.

The photographs of Figures 39 and 40 show the recommended mounting positions for a two rake configuration for two different aircraft.

The wake rake is still potentially an excellent flight test instrument. This test was hampered by the lack of static pressure information in the slipstream but still managed to illustrate the validity of the method. Recommendations for use are: decrease the number of rakes to 2 but increase the number of pressure measurements per rake and alternate static pressure measurements with total pressure measurements on the rake. The information available will then permit use of the linear momentum expression without the approximations which should yield a true value of thrust.

REFERENCES

1. Fage, A., "A Note on the Method of Estimation from Observations of Total Head, the Total Thrust of an Airscrew," British Reports and Memoranda No. 600, October 1922.

2. John, J. E. A., Gas Dynamics, Allyn and Bacon, Inc., 1969.

3. Milne-Thomson, L. M., "Theoretical Hydrodynamics," Macmillan, London, 1950.

4. Miley, S. J., Personal Communication on Rake Configuration and Probe Calibration.

5. Stickle, G. W., "Measurement of the Differential and Total Thrust and Torque of Six Full-Scale Adjustable-Pitch Propellers," NACA Report No. 421, 1932.

6. Vogeley, A. W., "Flight Measurement of Compressibility Effect on a Three-Blade Thin Clark-Y Propeller Operating at Constant Advance-Diameter Ratio and Blade Angle," NACA WR L-505, 1943.

7. Vogeley, A. W., "Climb and High-Speed Tests of a Curtiss No. 714-1C2-12 Four Blade Propeller on the Republic P-47C Airplane," NACA WR L-177, 1944.

8. Wright, M. A., "The Evaluation of a Simplified Form of Presentation for Five-Hole Spherical and Hemispherical Pitometer Calibration Data," Journal of Physics E.: Scientific Instruments, Vol. 3, 1970.

9. McCormick, B. W., Aerodynamics, Aeronautics, and Flight Mechanics, John Wiley and Sons, New York, 1979.

10. Brady, G. W., "Flight Testing with a Propeller Thrustmeter," SAE Journal, Vol. 52, No. 7, July 1944.

11. Openheim, H. E., "Flight Test Comparison of Propellers Using Clark-Y, NACA Series 16 and Combination Combination Clark-Y and NACA Series 16 Blade Profiles," Curtis-Wright Corporation Report No. C-1415, April 1943.

12. Leslie, E. P. and Woods, B. M., "The Effect of Slipstream Obstructions on Air Propellers," NACA Report No. 177, 1924.

13. Miley, S. J. and Hall, K. R., "Investigation of a Flight Test Method for the Measurement of Propeller Thrust," to be presented at the 1981 Business Aircraft Meeting and Exposition as SAE Paper No. 810603, 1981.

PROBE	LOC.	r/R
S1	26.2	1.20
K1	22.6	1.10
K2	20.8	1.05
K3	19.9	1.025
S2	19.0	1.00
K4	18.1	0.975
K5	17.2	0.95
K6	16.3	0.925
K7	15.4	0.90
K8	13.6	0.85
S3	11.8	0.80
K9	10.0	0.75
K10	8.2	0.70
S4	4.6	0.60
K11	1.0	0.50

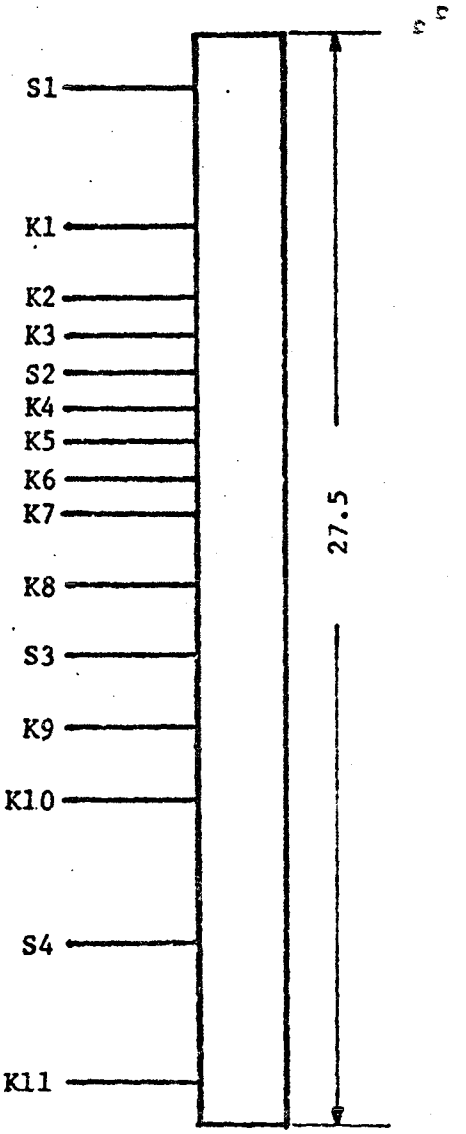

K12	6.4	0.40

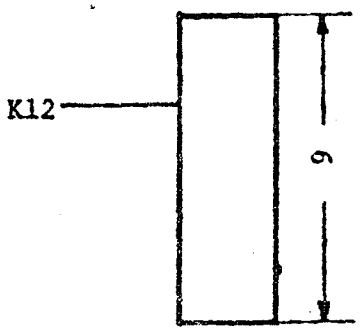

Dimension : Inch

Figure 1 Construction of Wake Survey Rake

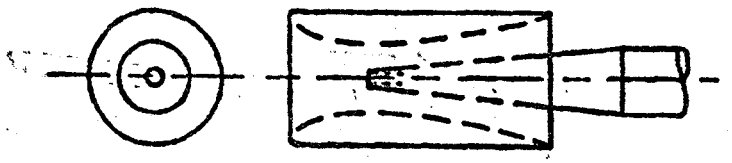

a. Kiel Tube

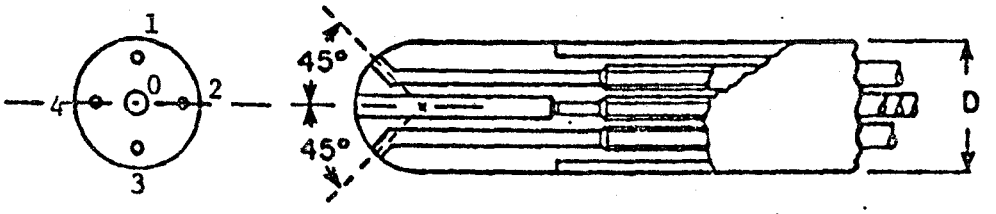

b. Directional Pitot-Static-Tube Head

Figure 2 Configuration of Kiel and 5-Hole Probes

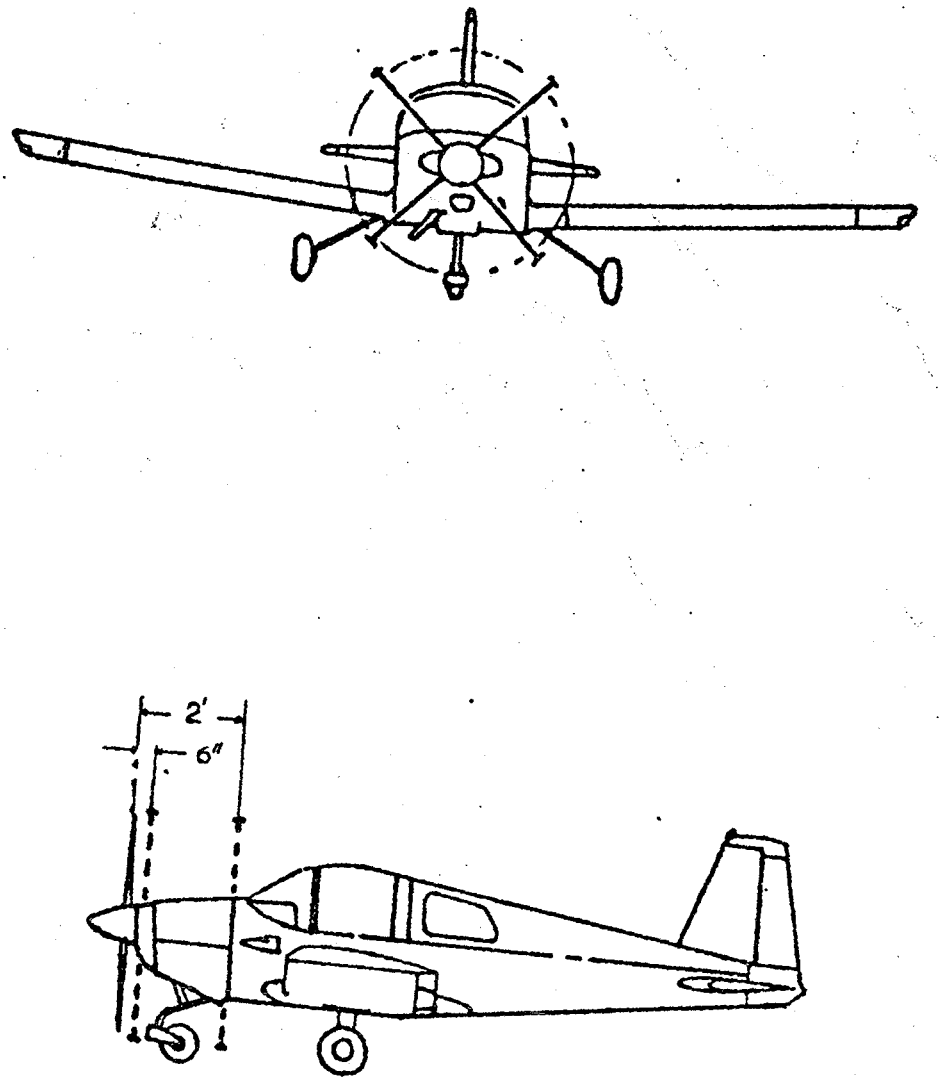

Figure 3 Mounting Position of Wake Survey Rake

PURPOSE	CONFIGURATION	INDEPENDENT VARIABLES
Drag Polar	*Propeller off/Inlets Open	V-Appropriate Speed; α Sweep
Drag Polar	Propeller off/Inlets Closed	V-Appropriate Speed; α Sweep
Drag Polar	Propeller off/Inlets Closed/Wake Rake	V-Appropriate Speed; α Sweep
Drag Polar	Propeller Fixed/Inlets Open	V-Appropriate Speed; α Sweep
**Thrust Matrix	Wake Survey Rake Aft	J and C_p-Available Range; α = 0°
		J and C_p-Available Range; α = 4°
		J and C_p-Available Range; α = 8°
		J and C_p-Available Range; α = 12°
**Thrust Matrix	Wake Survey Rake Forward	
**Thrust Matrix	No Wake Survey Rake	
	Boundary Layer Mice	

Notes: J - Advance Ratio
C_p - Power Coefficient
*Spinner Installed
**Matrix of Independent Variables is Identical

Figure 4 Wind Tunnel Test Plan

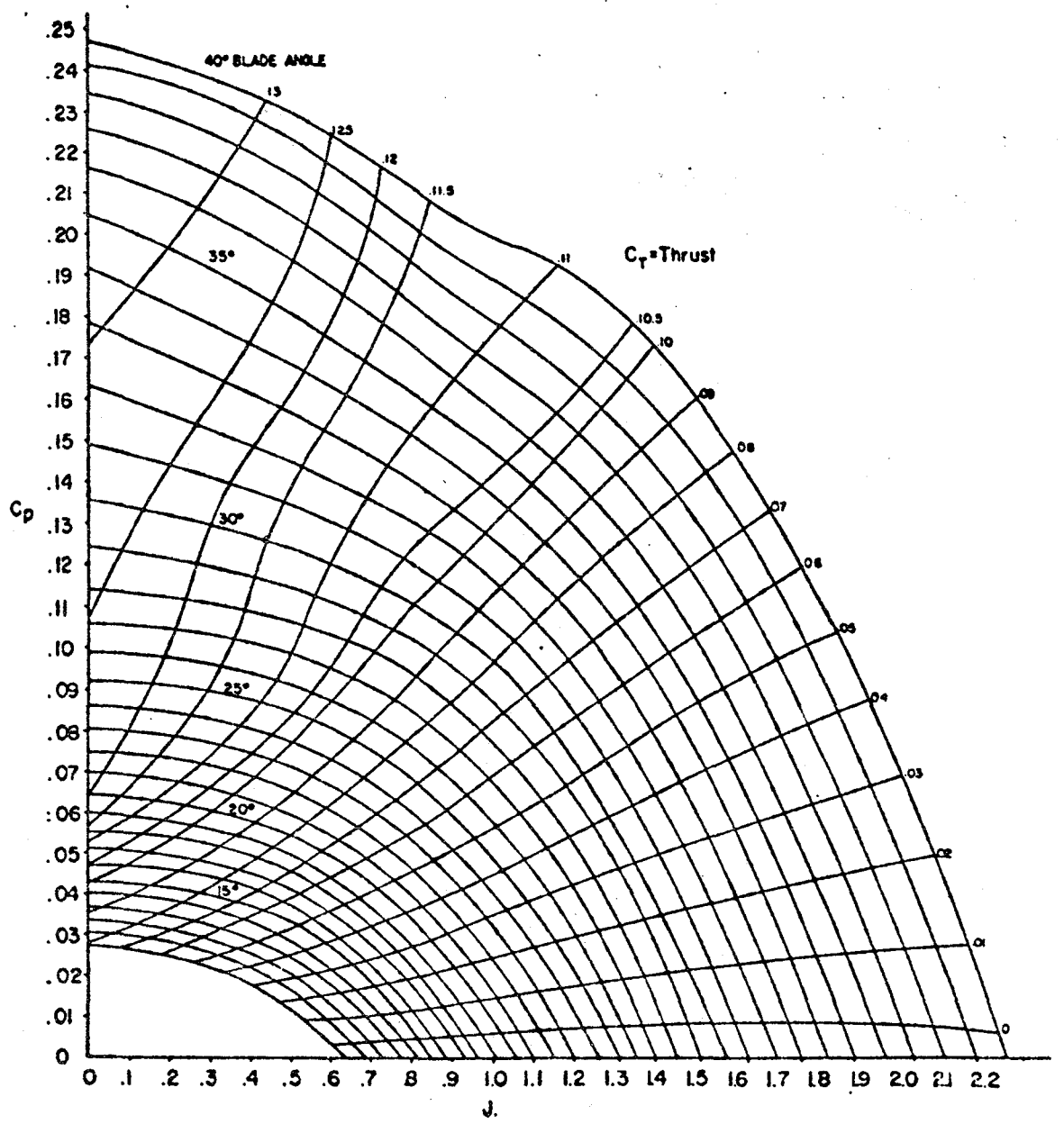

Figure 5 NACA Gray Chart. Coefficient of Power versus Advance Ratio

	$\beta_{.75} = 18.8°$			$\beta_{.75} = 15.4°$		
J	η	C_p	C_t	η	C_p	C_t
.20	.42	.0570	.1197	.47	.0458	.1076
.25	.52	.0558	.1160	.56	.0430	.0963
.30	.59	.0540	.1006	.64	.0420	.0896
.35	.65	.0530	.0984	.72	.0405	.0833
.40	.71	.0520	.0923	.79	.0390	.0770
.45	.76	.0500	.0844	.84	.0370	.0691
.50	.80	.0480	.0772	.89	.0350	.0623
.55	.83	.0465	.0702	.93	.0325	.0547
.60	.85	.0435	.0616	.95	.0280	.0443
.65	.87	.0400	.0535	.94	.0250	.0362
.70	.88	.0360	.0453	.91	.0210	.0273
.75	.885	.0310	.0364	.835	.0150	.0167

Table 6 Theoretical C_t of Installed Propeller on Yankee

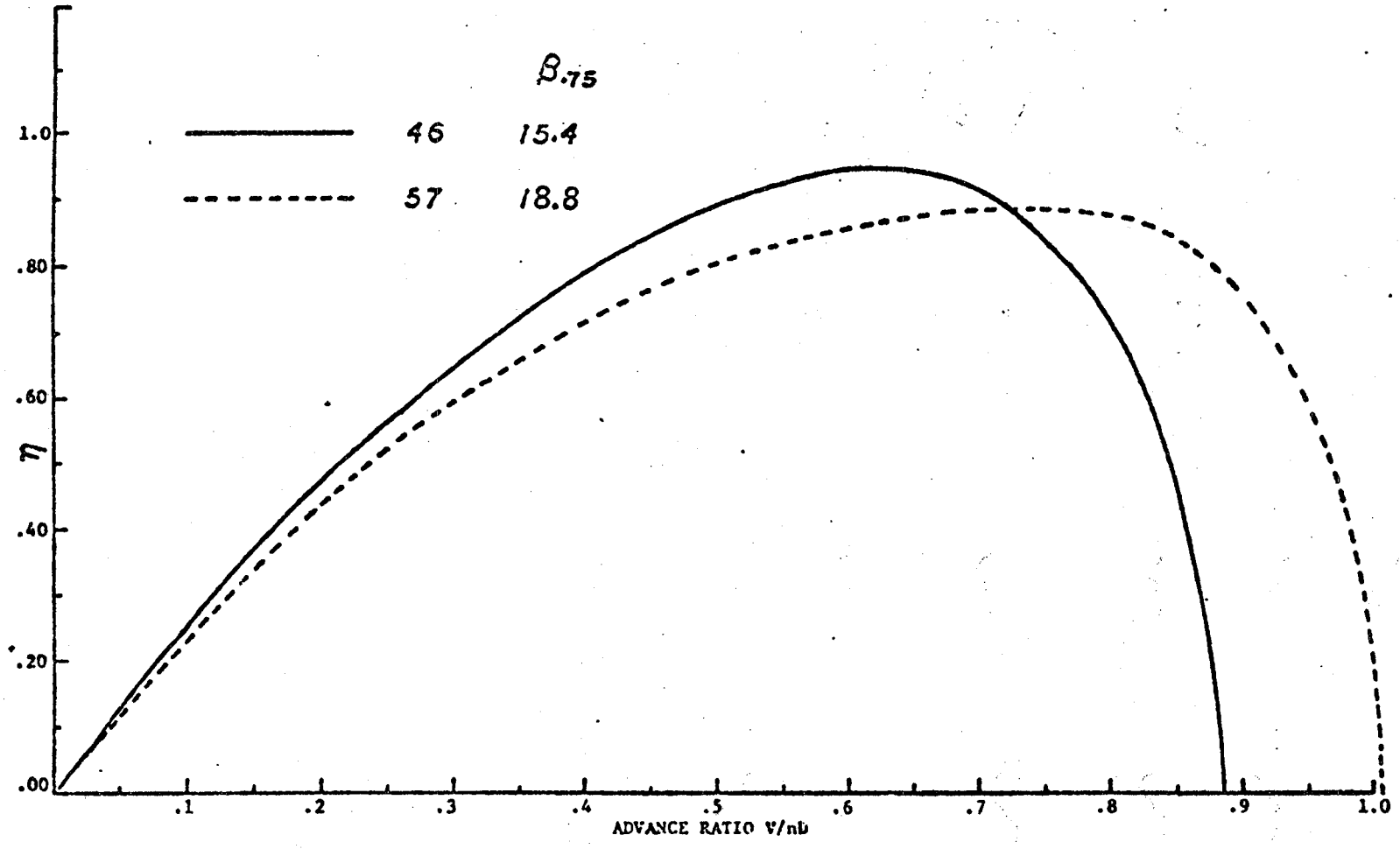

Figure 7 Yankee Installed Propeller Efficiency

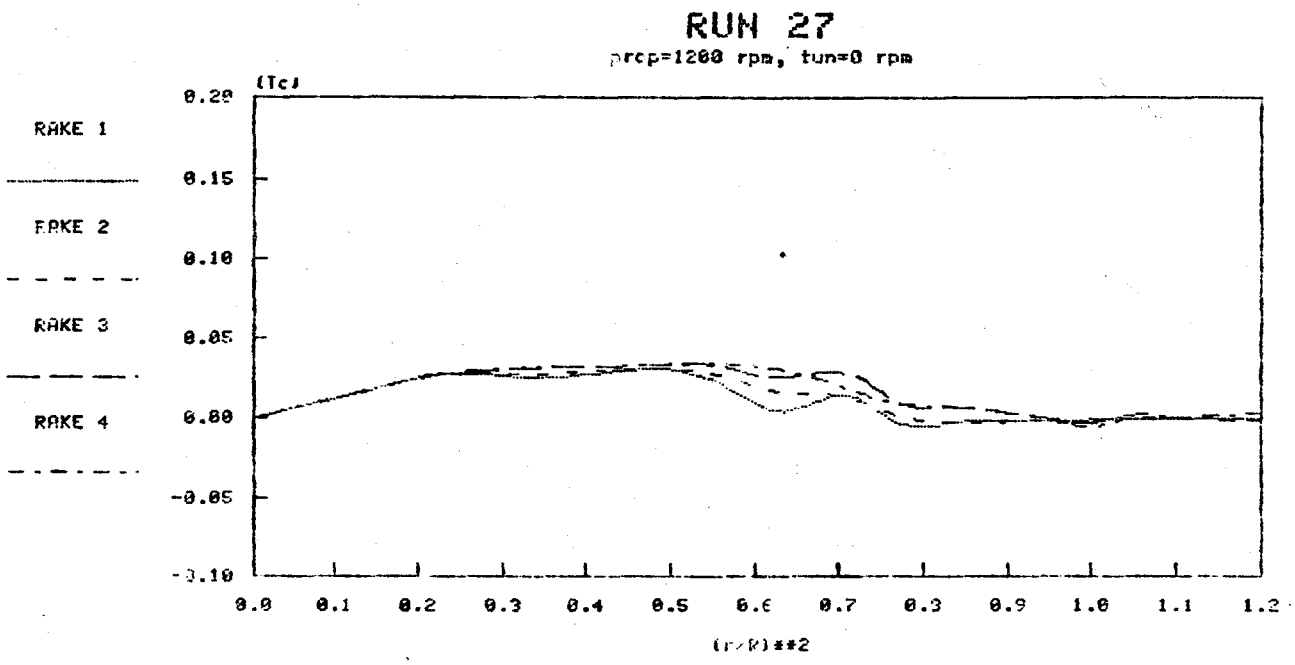

Figure 8 Thrust Coefficient Distribution for Run 27

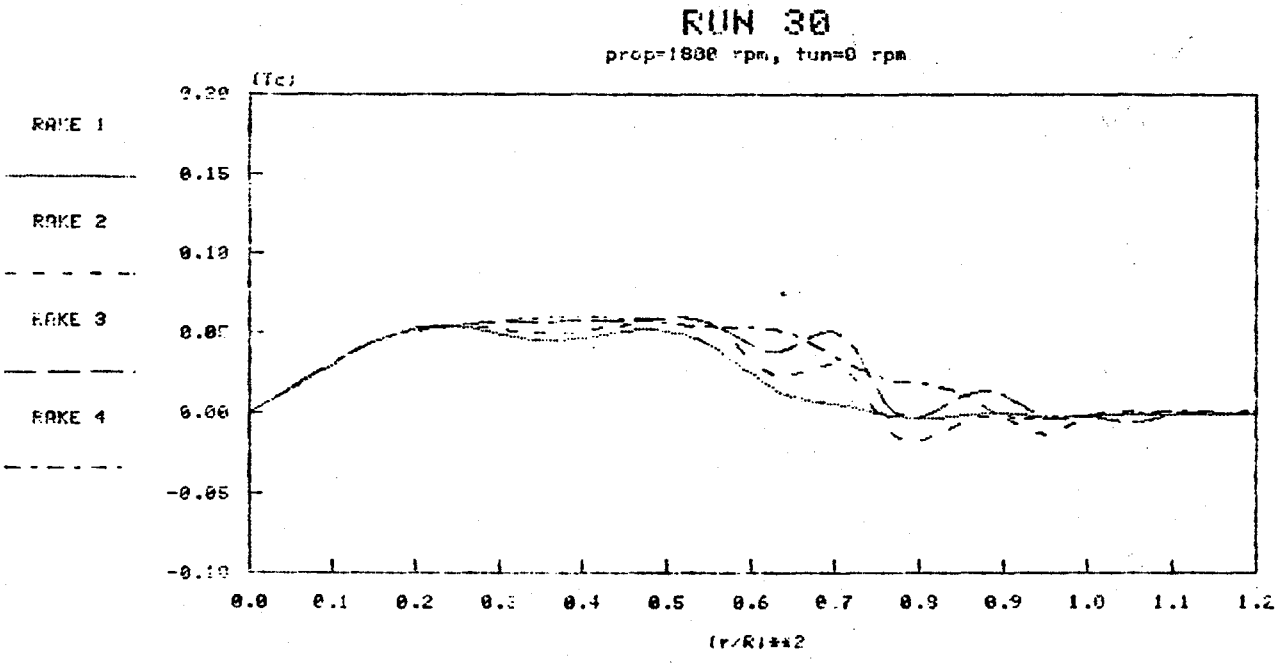

Figure 9 Thrust Coefficient Distribution for Run 30

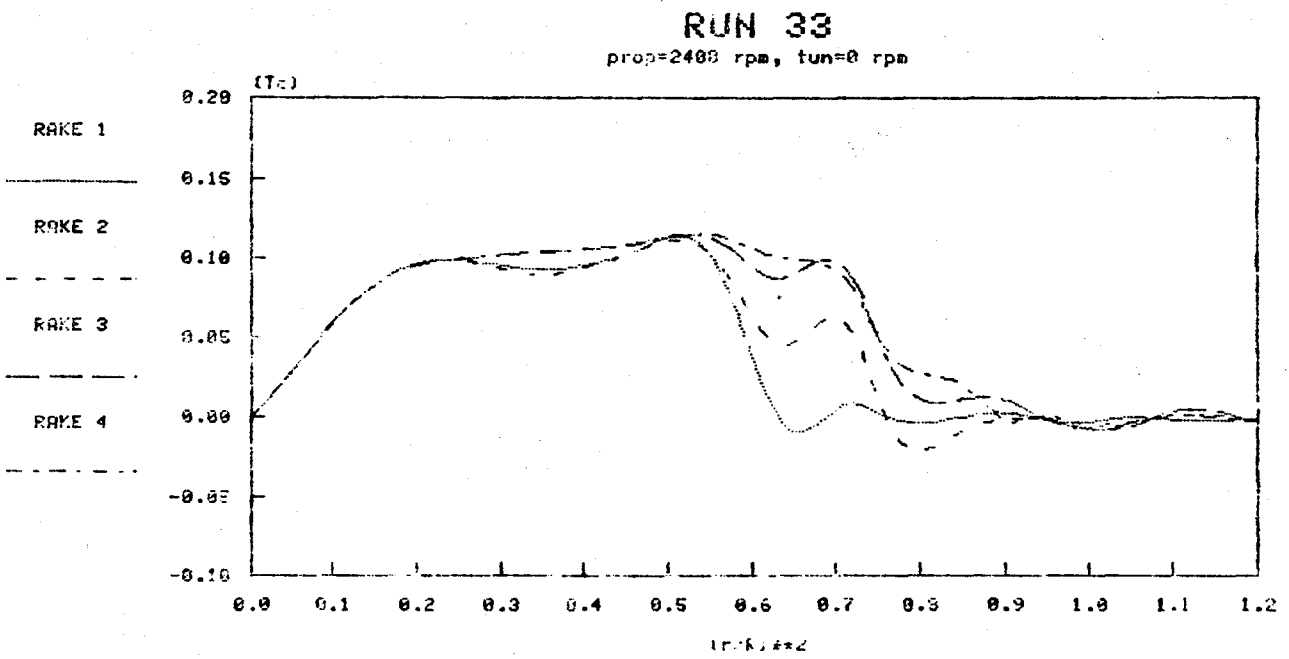

Figure 10 Thrust Coefficient Distribution for Run 33

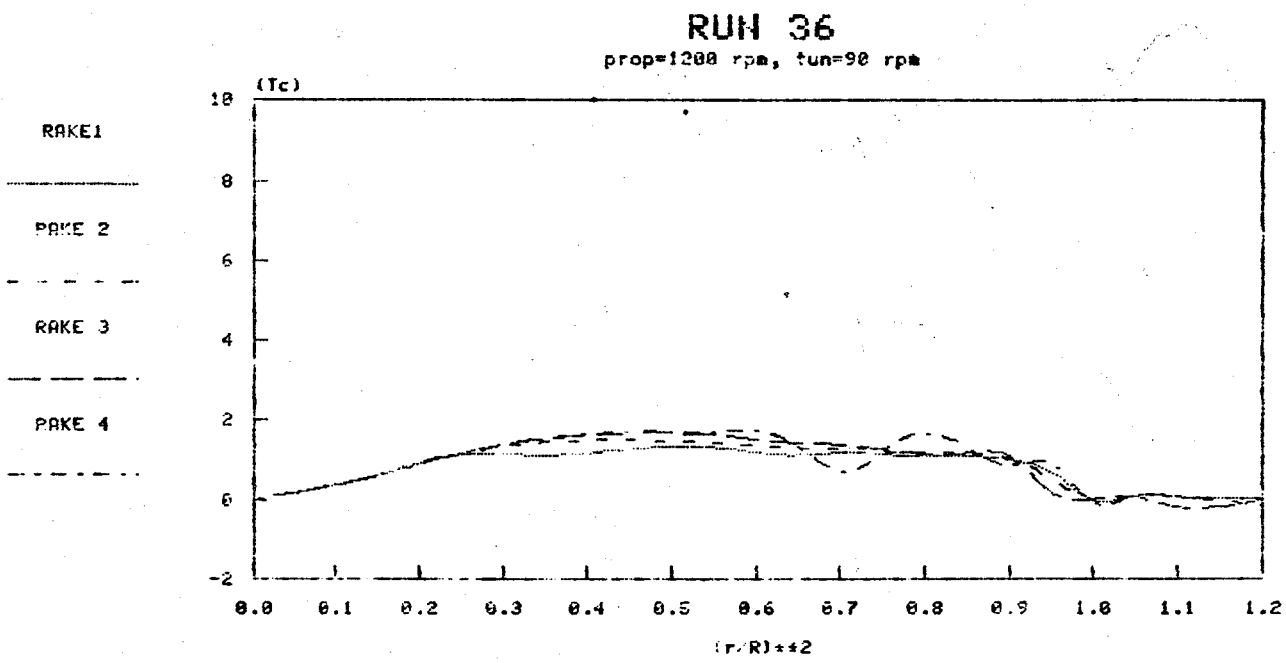

Figure 11 Thrust Coefficient Distribution for Run 36

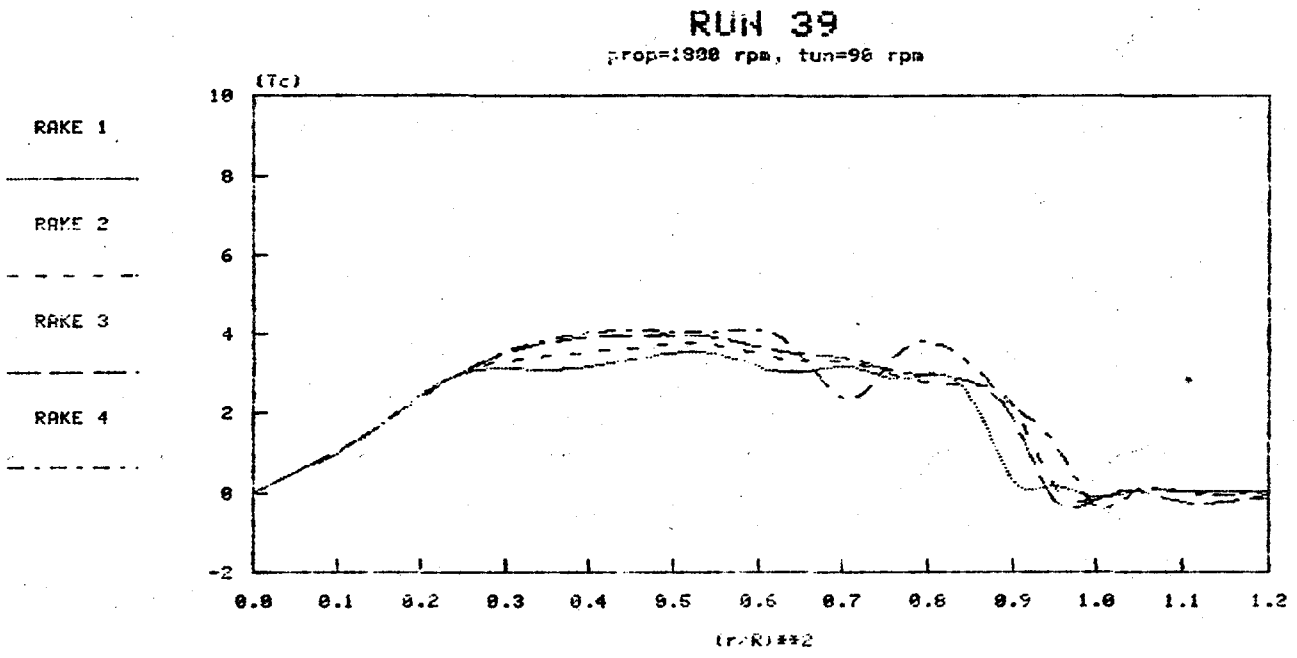

Figure 12 Thrust Coefficient Distribution for Run 39

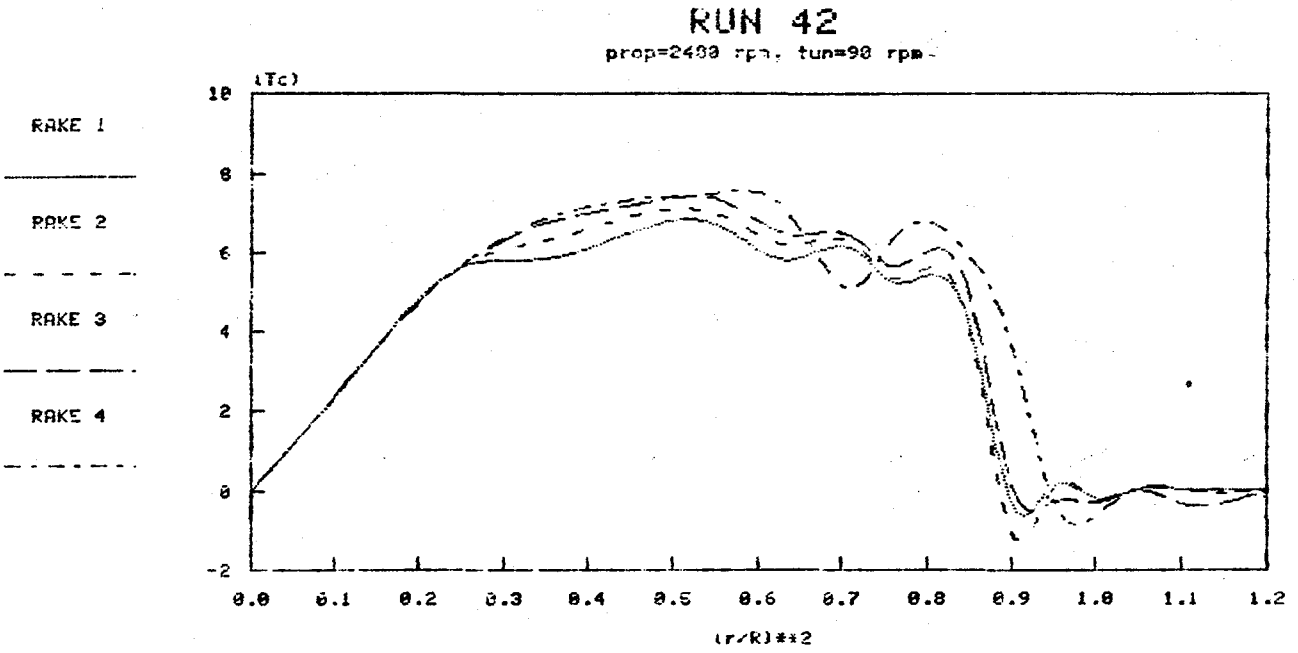

Figure 13 Thrust Coefficient Distribution for Run 42

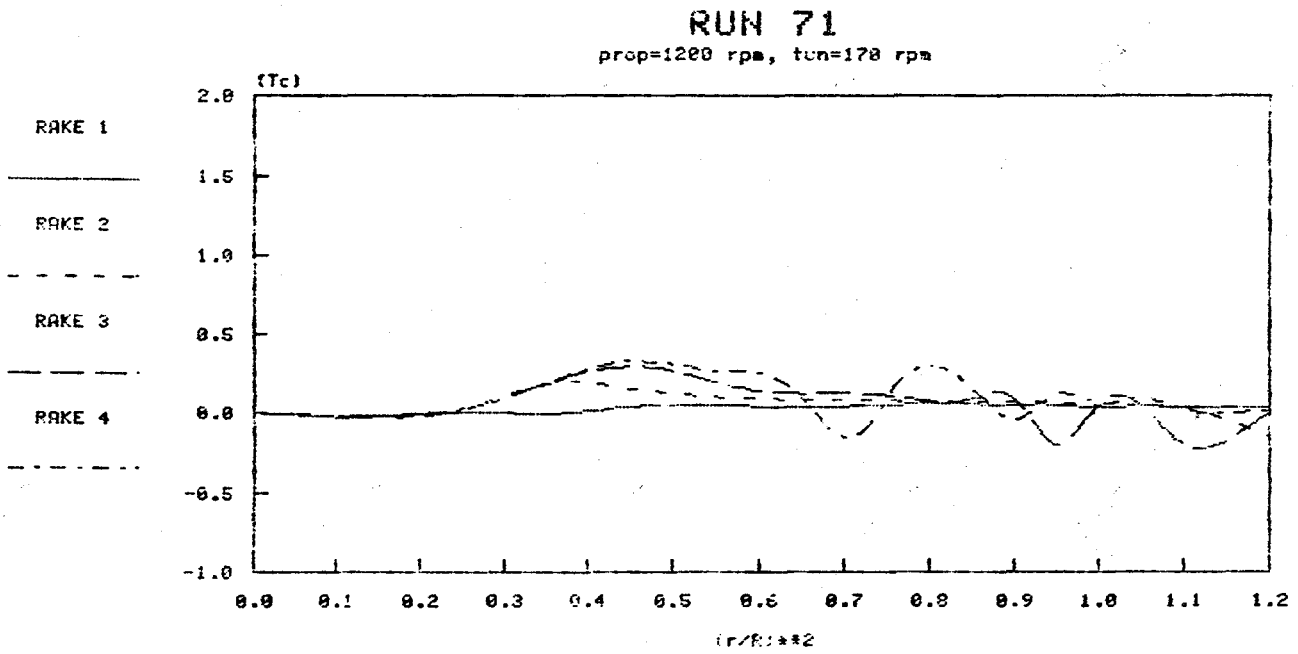

Figure 14 Thrust Coefficient Distribution for Run 71

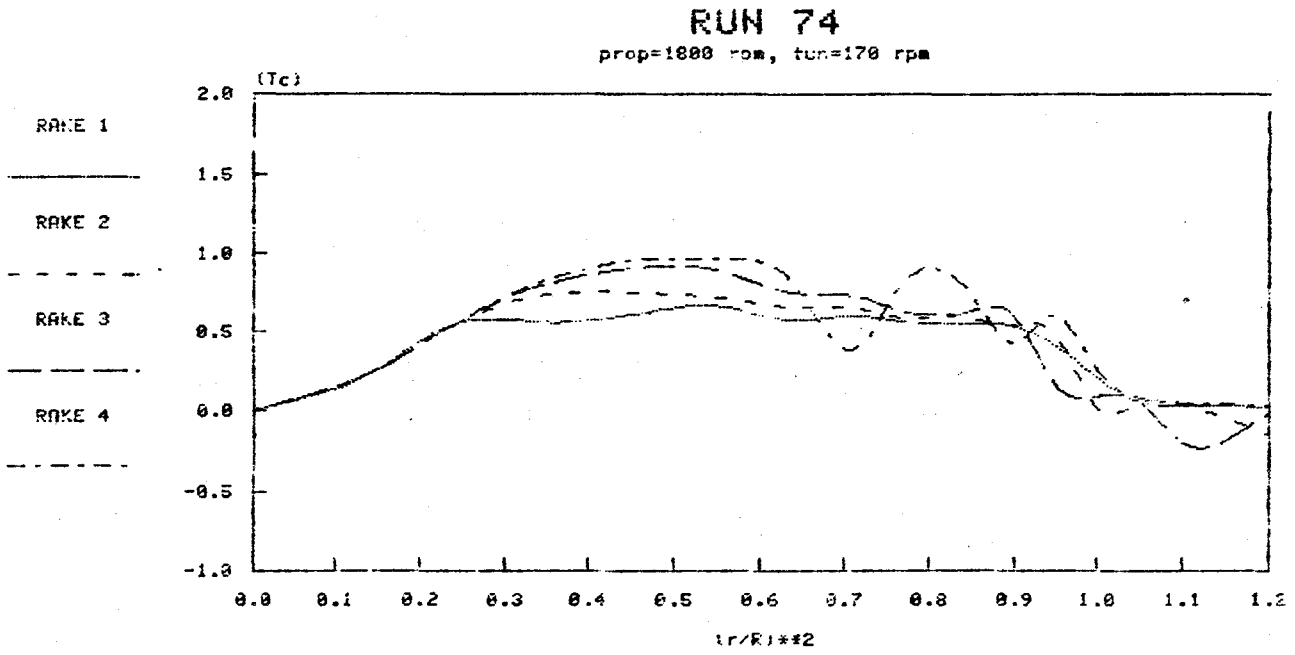

Figure 15 Thrust Coefficient Distribution for Run 74

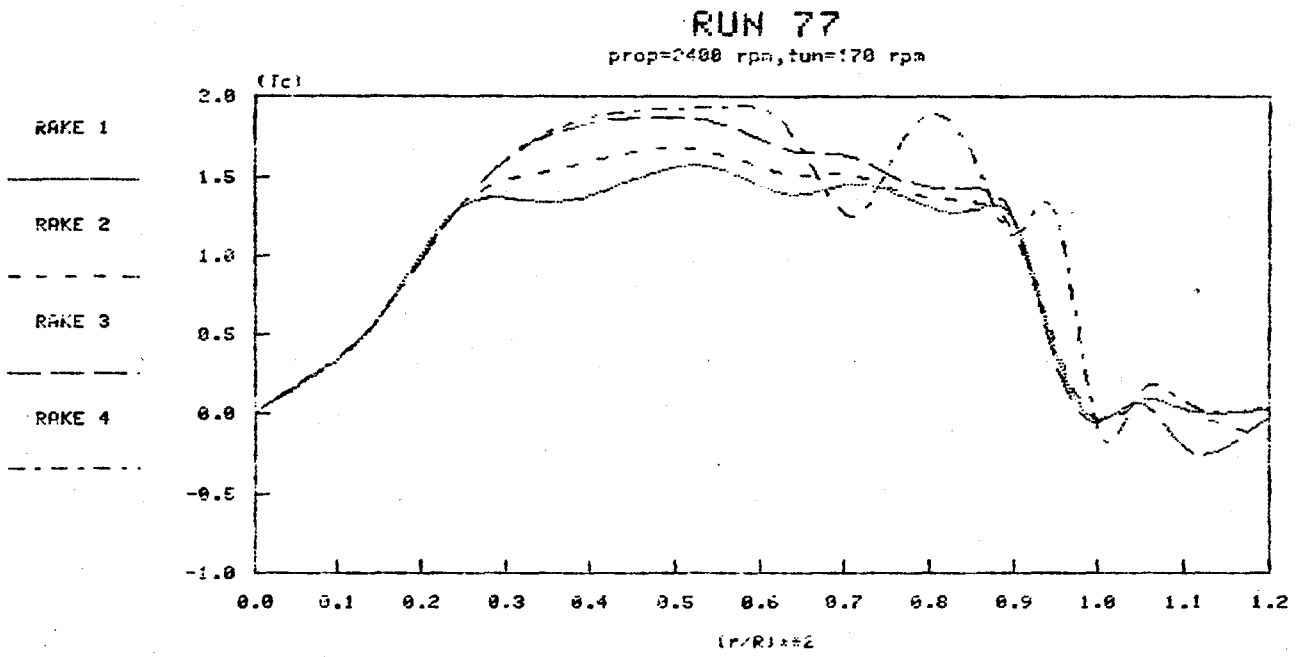

Figure 16 Thrust Coefficient Distribution for Run 77

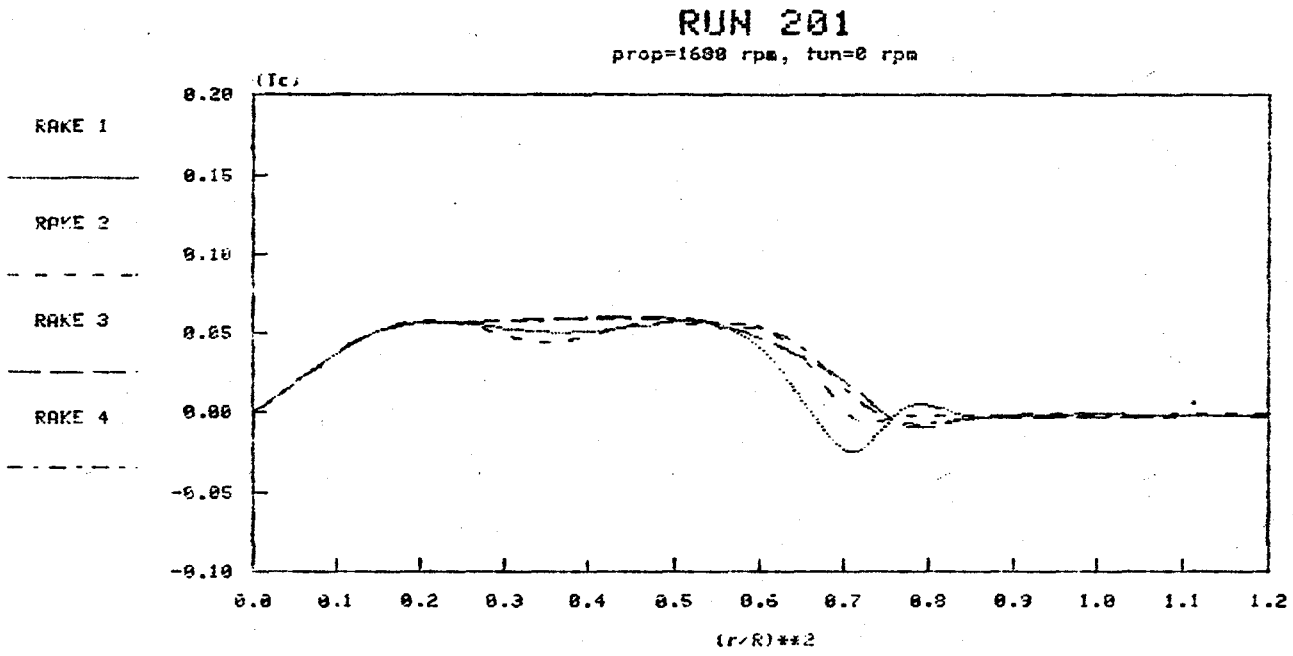

Figure 17 Thrust Coefficient Distribution for Run 201

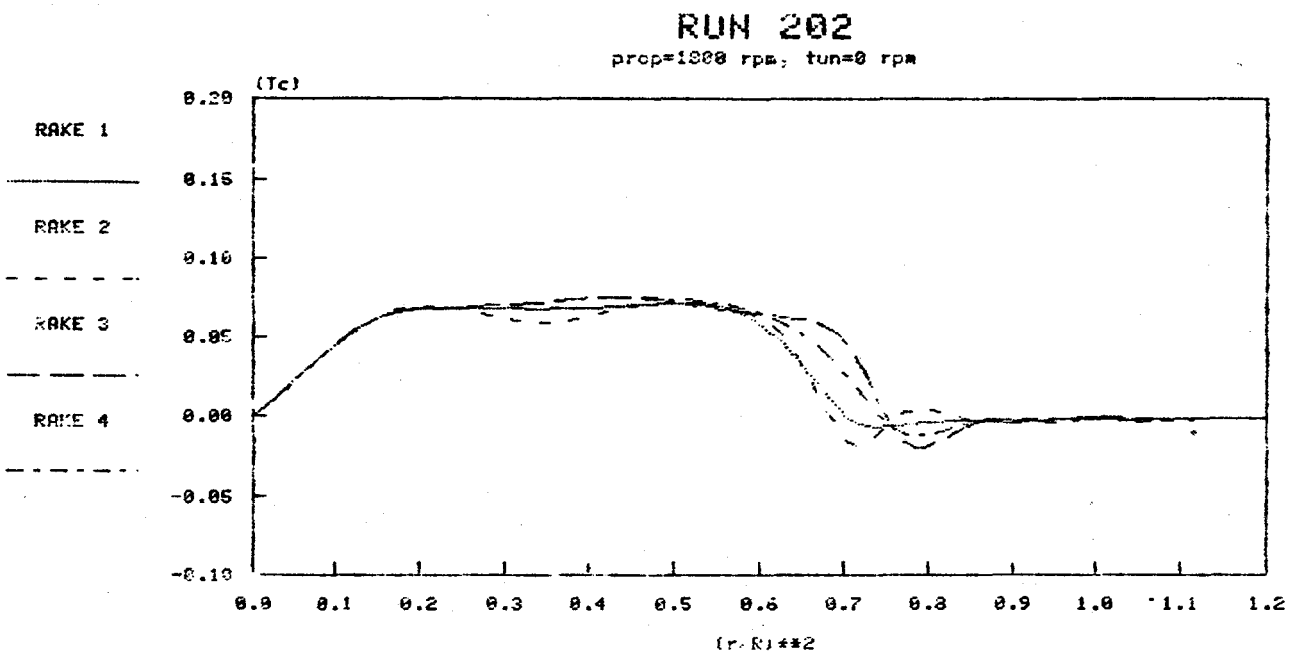

Figure 18 Thrust Coefficient Distribution for Run 202

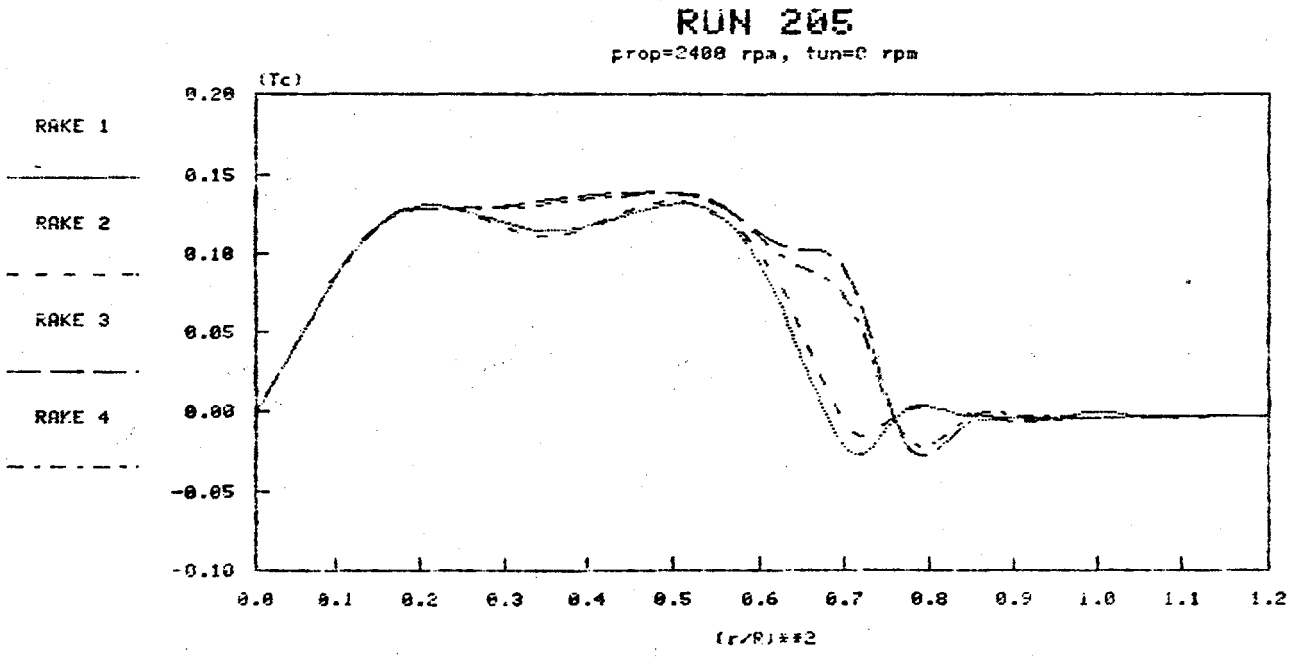

Figure 19 Thrust Coefficient Distribution for Run 205

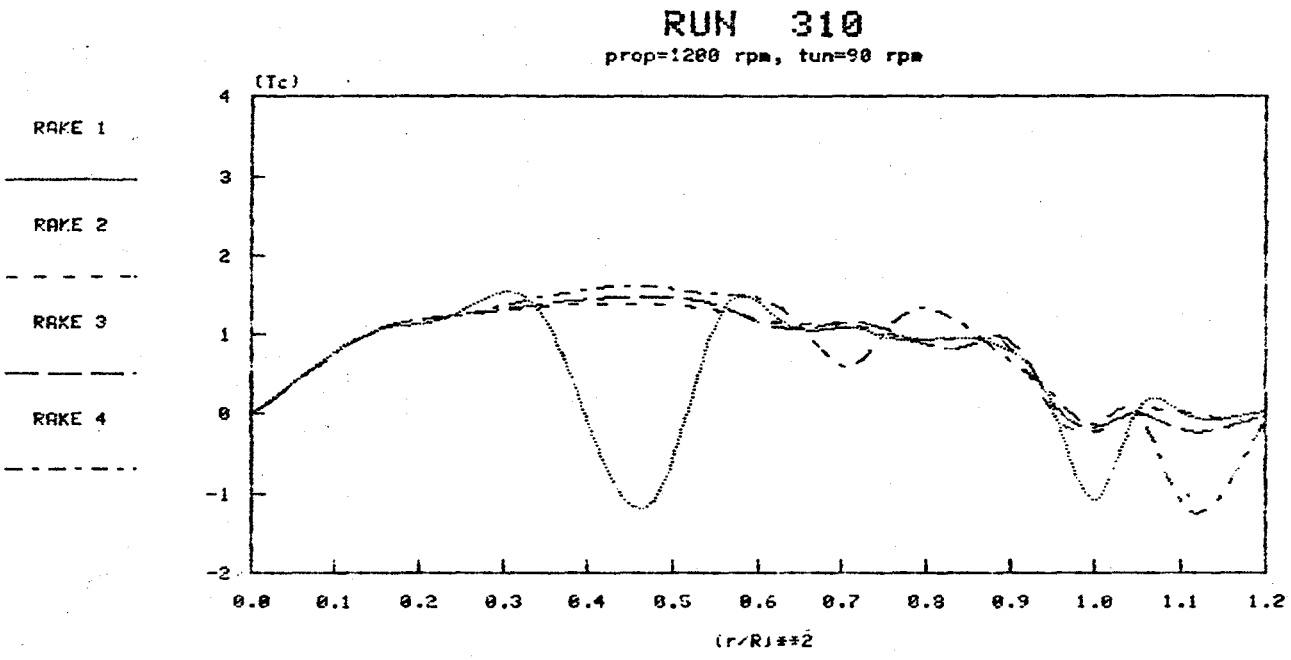

Figure 20 Thrust Coefficient Distribution for Run 310

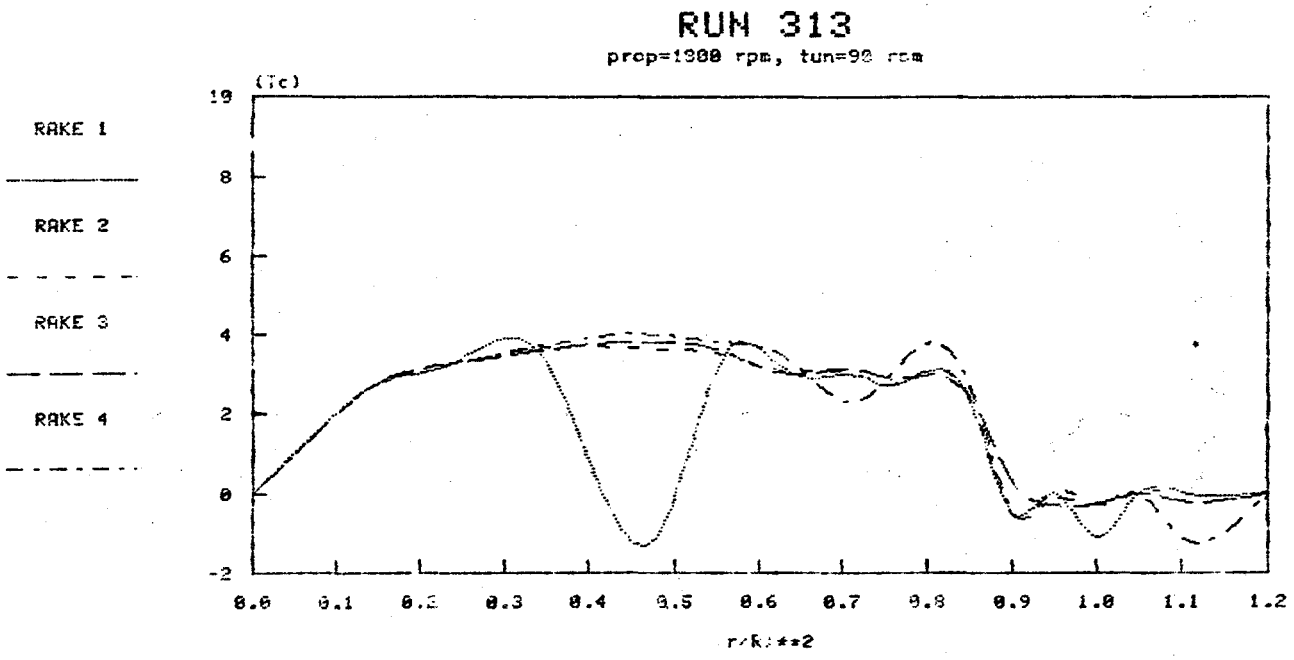

Figure 21 Thrust Coefficient Distribution for Run 313

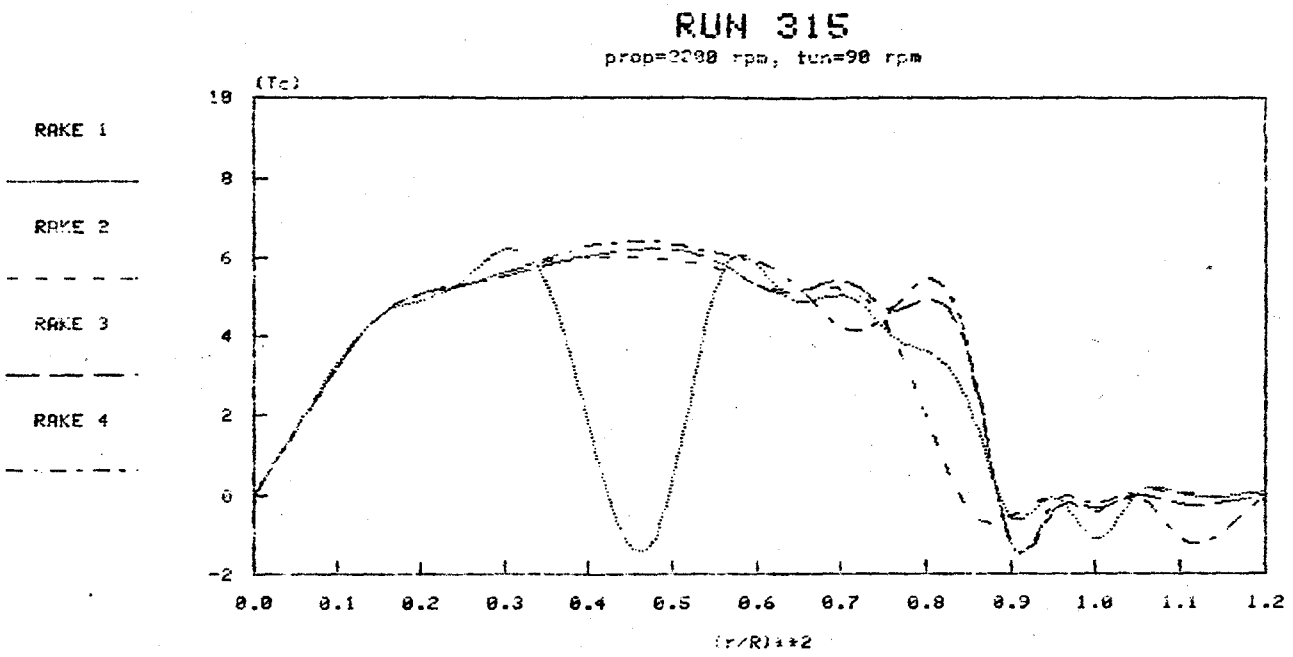

Figure 22 Thrust Coefficient Distribution for Run 315

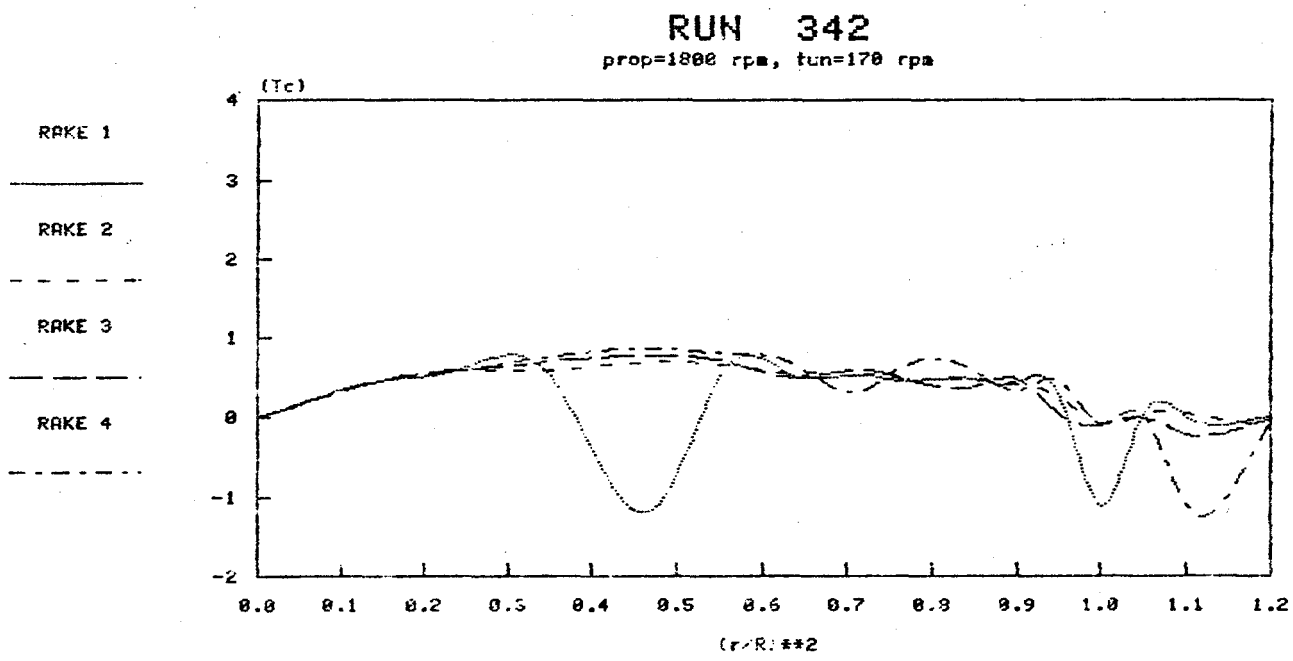

Figure 23 Thrust Coefficient Distribution for Run 342

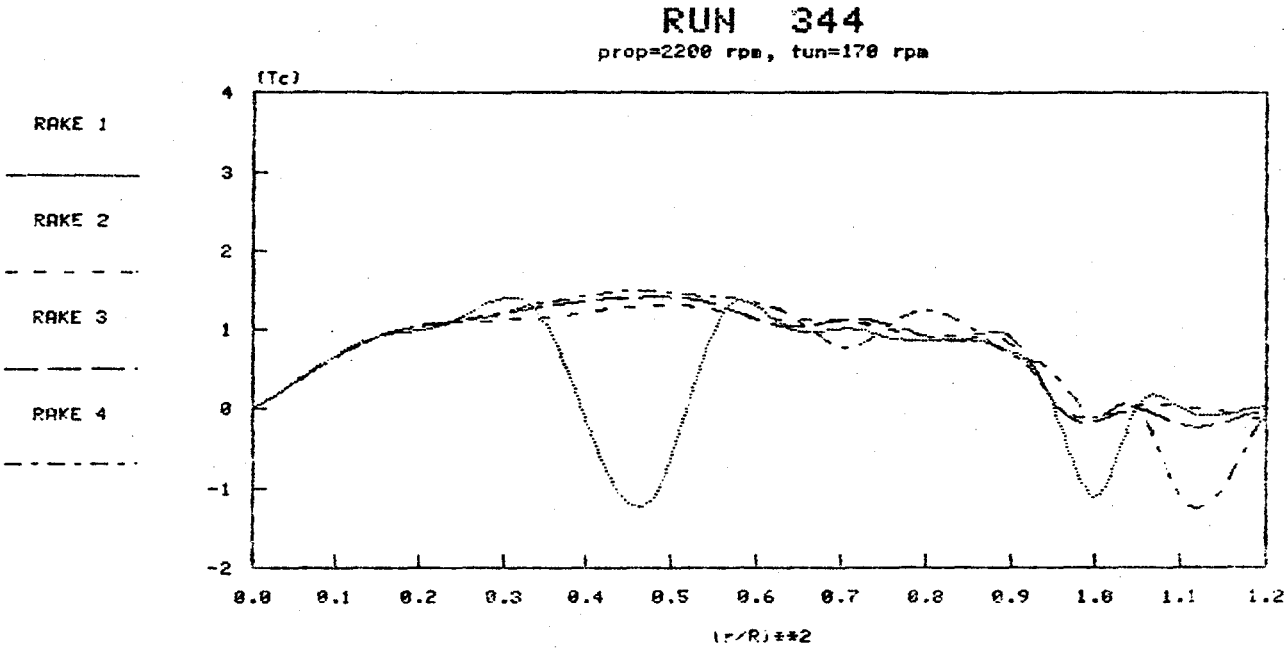

Figure 24 Thrust Coefficient Distribution for Run 344

RUN	QBR	VEL	RPM	TRQ	THB	ETA	J	CT	CP	THR	CTR	ETAR
27.	.00	.0	1187.	17.3	87.6	.00	.000	.081	.017	72.2	.063	.000
30.	.00	.0	1562.	33.3	172.9	.00	.000	.093	.019	133.1	.067	.000
33.	.00	.0	2147.	73.8	358.5	.00	.000	.102	.022	256.7	.069	.000
36.	2.34	45.5	1181.	29.3	82.9	1.04	.390	.077	.029	70.5	.062	.845
39.	2.46	46.7	1764.	62.8	220.4	.89	.268	.092	.028	179.4	.071	.688
42.	2.55	47.5	2355.	113.9	424.2	.72	.204	.099	.023	335.2	.075	.540
71.	8.38	86.7	1158.	12.0	29.7	1.76	.758	.029	.012	20.8	.019	1.164
74.	8.44	86.9	1776.	54.7	155.5	1.33	.496	.065	.029	134.4	.053	.895
77.	8.51	87.3	2357.	110.0	337.8	1.09	.376	.080	.028	292.8	.065	.886
105.	8.37	87.3	0.	.5	.5	.00	.000	.000	.000	-1.9	.000	.000
129.	2.44	46.5	1184.	27.3	78.9	1.09	.398	.073	.027	70.8	.062	.924
130.	2.45	46.6	1377.	42.5	112.4	.85	.343	.077	.031	102.5	.067	.740
131.	2.47	46.9	1579.	61.2	153.9	.71	.301	.080	.034	146.1	.072	.644
201.	.00	.0	1578.	50.7	194.8	.00	.000	.101	.028	125.8	.062	.000
202.	.00	.0	1751.	69.1	243.8	.00	.000	.102	.031	156.6	.063	.000
205.	.00	.0	2348.	164.8	448.0	.00	.000	.105	.041	294.3	.066	.000
313.	2.39	45.9	1760.	75.1	196.1	.65	.264	.082	.033	168.1	.067	.533
315.	2.44	46.4	2171.	115.6	326.4	.58	.217	.089	.034	267.7	.070	.451
369.	.00	.0	1763.	634.5	229.4	.00	.000	.098	.288	143.2	.057	.000
367.	.00	.0	2173.	520.6	376.3	.00	.000	.106	.156	237.8	.062	.000
372.	.00	.0	1178.	634.6	98.5	.00	.000	.094	.645	65.8	.059	.000
344.	8.50	86.6	2177.	109.5	251.2	.87	.403	.069	.032	215.3	.056	.714
342.	8.44	86.3	1768.	72.1	131.9	.85	.494	.055	.032	109.9	.043	.681
339.	8.42	86.2	1193.	23.7	22.1	.64	.732	.020	.023	4.6	.004	.127
310.	2.33	45.4	1178.	32.0	69.7	.80	.391	.065	.032	62.6	.056	.681
311.	2.35	45.6	1384.	45.2	107.7	.75	.333	.073	.032	95.5	.062	.637
312.	2.37	45.7	1572.	59.3	149.0	.70	.295	.078	.033	129.8	.065	.582
343.	8.48	86.5	1980.	94.1	188.8	.84	.442	.062	.033	158.8	.050	.674

Figure 25 Summary of Results in lb/ft/sec Units
Standard Units lb/ft/sec

RUN	QBR	VEL	RPM	TRQ	THB	ETA	J	CT	CP	THR	CTR	ETAR
27.	0.	.0	1187.	23.5	390.	.00	.000	.081	.017	321.	.063	.000
30.	0.	.0	1562.	45.1	769.	.00	.000	.093	.019	592.	.067	.000
33.	0.	.0	2147.	100.1	1595.	.00	.000	.102	.022	1142.	.069	.000
36.	112.	13.9	1181.	39.7	369.	1.04	.390	.077	.029	314.	.062	.845
39.	118.	14.2	1764.	85.2	980.	.89	.268	.092	.028	798.	.071	.688
42.	122.	14.5	2355.	154.4	1887.	.72	.204	.099	.028	1491.	.075	.540
71.	401.	26.4	1158.	16.3	132.	1.76	.758	.029	.012	93.	.019	1.164
74.	404.	26.5	1776.	74.2	692.	1.33	.496	.065	.029	598.	.053	.895
77.	407.	26.6	2357.	149.1	1503.	1.09	.376	.080	.028	1302.	.065	.886
105.	401.	26.6	0.	.7	2.	.00	.000	.000	.000	-8.	.000	.000
129.	117.	14.2	1184.	37.0	351.	1.09	.398	.073	.027	315.	.062	.924
130.	117.	14.2	1377.	57.6	500.	.85	.343	.077	.031	456.	.067	.740
131.	118.	14.3	1579.	83.0	685.	.71	.301	.080	.034	650.	.072	.644
201.	0.	.0	1578.	68.7	866.	.00	.000	.101	.028	559.	.062	.000
202.	0.	.0	1751.	93.7	1084.	.00	.000	.102	.031	697.	.063	.000
205.	0.	.0	2348.	223.4	1993.	.00	.000	.105	.041	1309.	.066	.000
313.	114.	14.0	1760.	101.9	872.	.65	.264	.082	.033	748.	.067	.533
315.	117.	14.1	2171.	156.7	1452.	.58	.217	.089	.034	1191.	.070	.451
369.	0.	.0	1763.	860.2	1020.	.00	.000	.098	.288	637.	.057	.000
367.	0.	.0	2173.	705.8	1674.	.00	.000	.106	.156	1058.	.062	.000
372.	0.	.0	1178.	860.4	438.	.00	.000	.094	.645	293.	.059	.000
344.	407.	26.4	2177.	148.5	1117.	.87	.403	.069	.032	958.	.056	.714
342.	404.	26.3	1768.	97.7	587.	.85	.494	.055	.032	489.	.043	.681
339.	403.	26.3	1193.	32.1	98.	.64	.732	.020	.023	20.	.004	.127
310.	112.	13.8	1178.	43.4	310.	.80	.391	.065	.032	278.	.056	.681
311.	113.	13.9	1384.	61.3	479.	.75	.333	.073	.032	425.	.062	.637
312.	113.	13.9	1572.	80.4	663.	.70	.295	.078	.033	577.	.065	.582
343.	406.	26.4	1980.	127.6	840.	.84	.442	.062	.033	706.	.050	.674

Figure 26 Summary of Results in n/m/sec Unit
SI Units n/m/sec

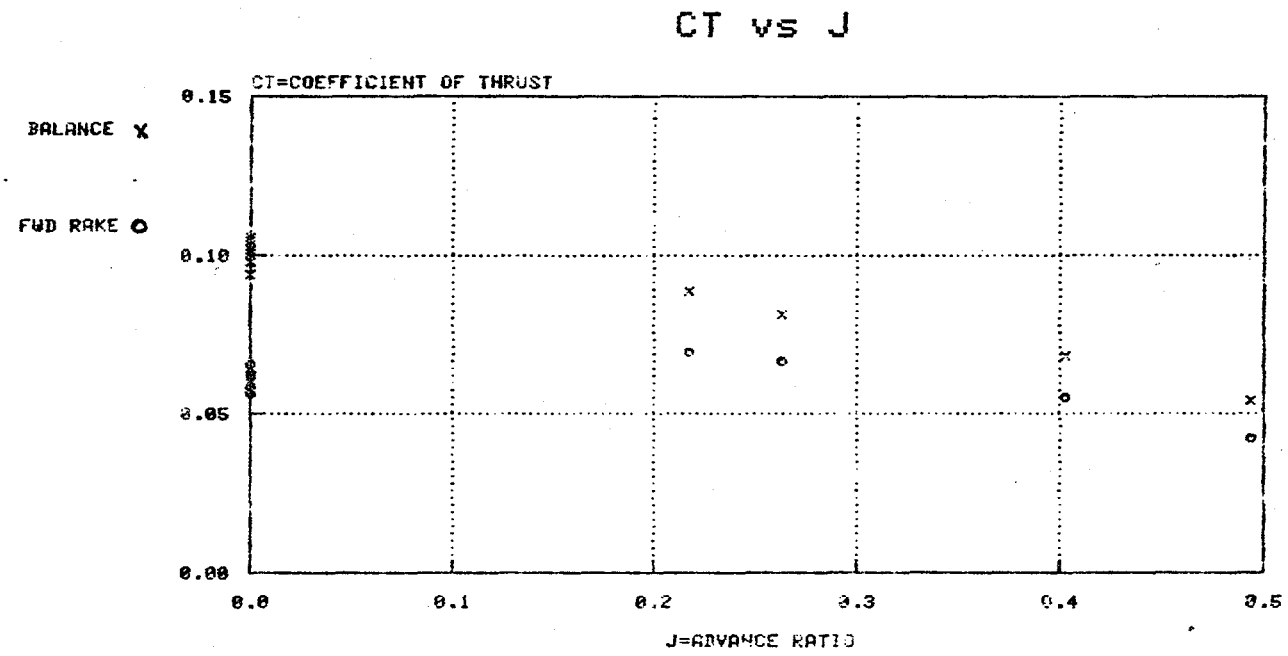

Figure 27 CT vs J for forward rake

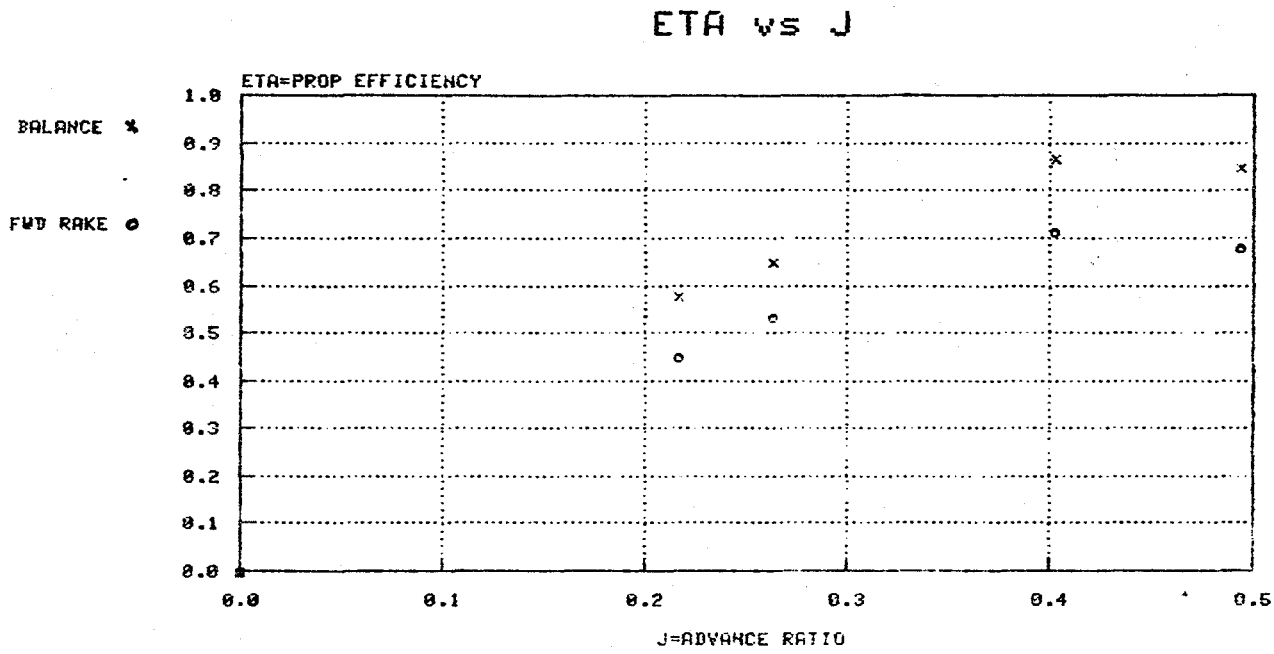

Figure 28 ETA vs J for forward rake

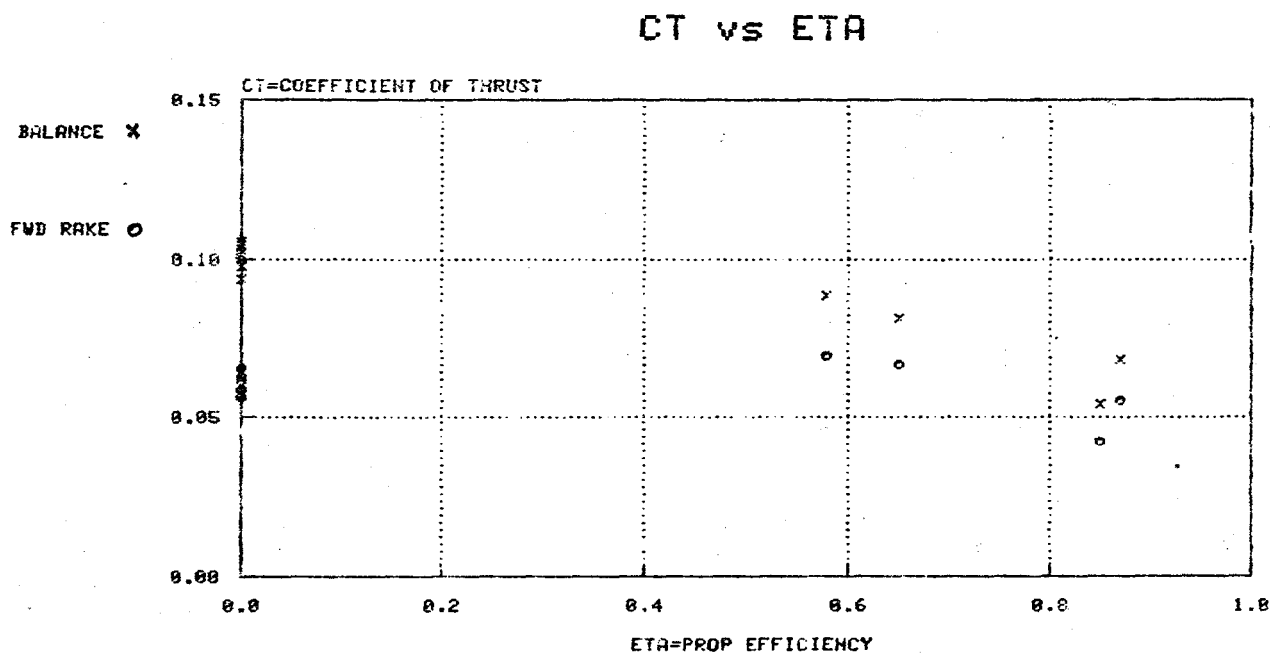

Figure 29 CT vs ETA for forward rake

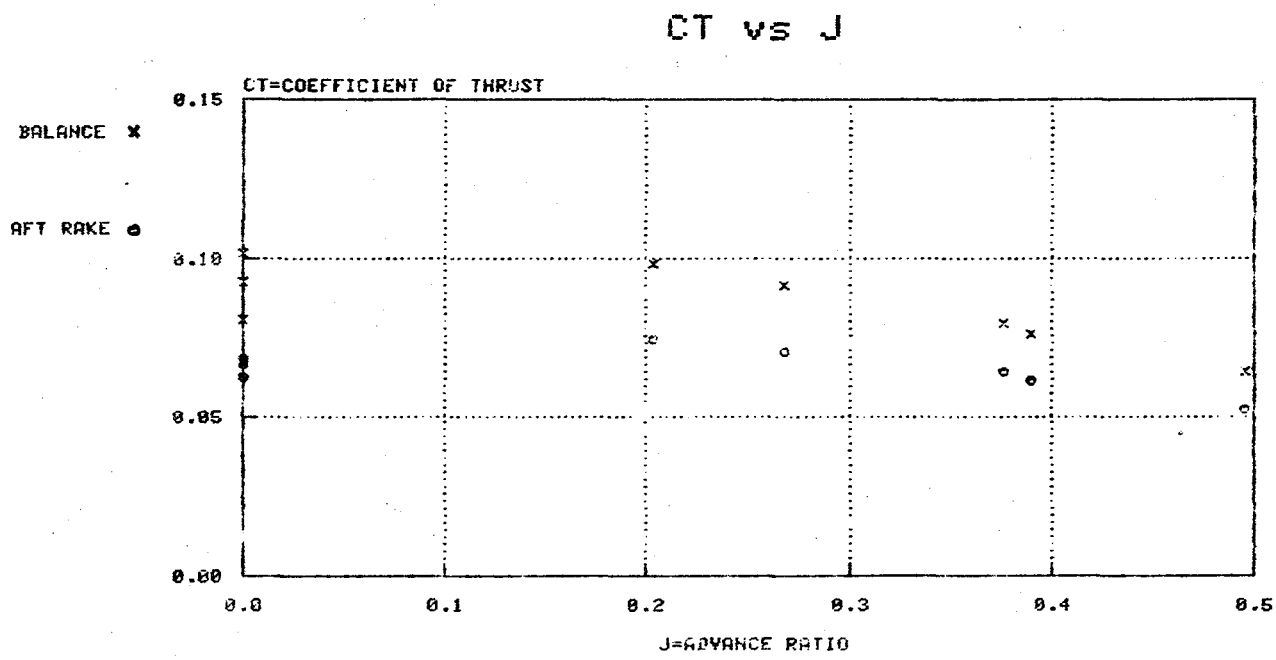

Figure 30 CT vs J for Aft Rake

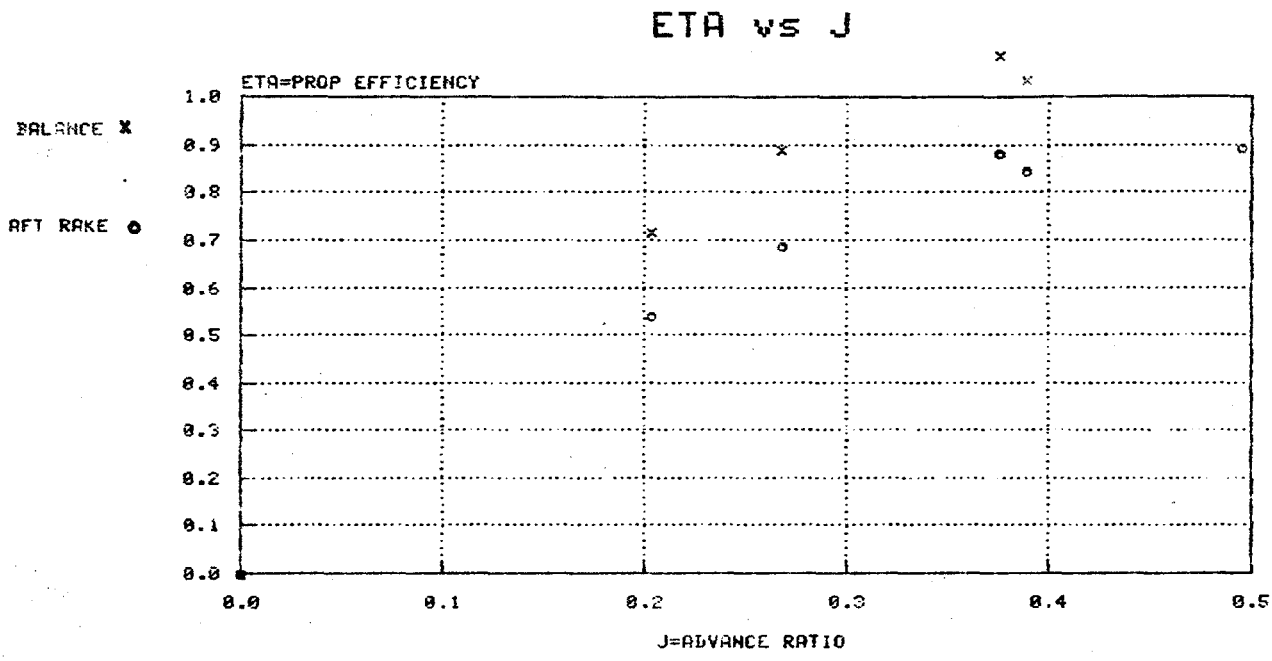

Figure 31 ETA vs J for Aft Rake

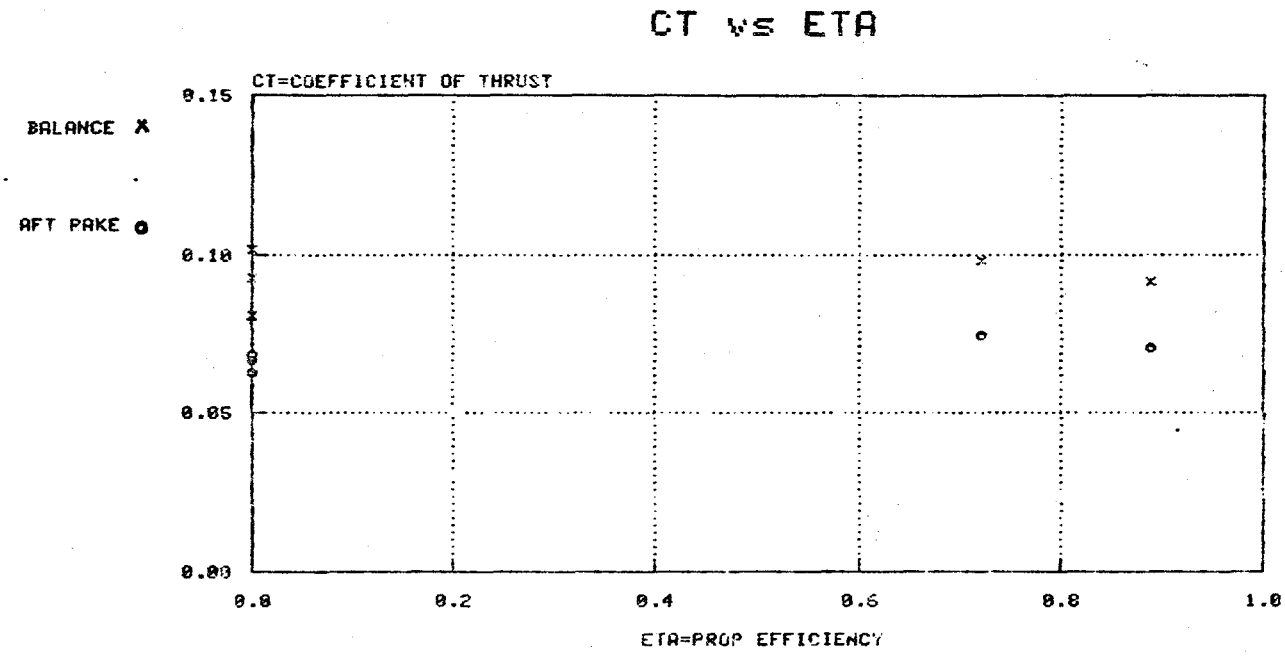

Figure 32 CT vs ETA for Aft Rake

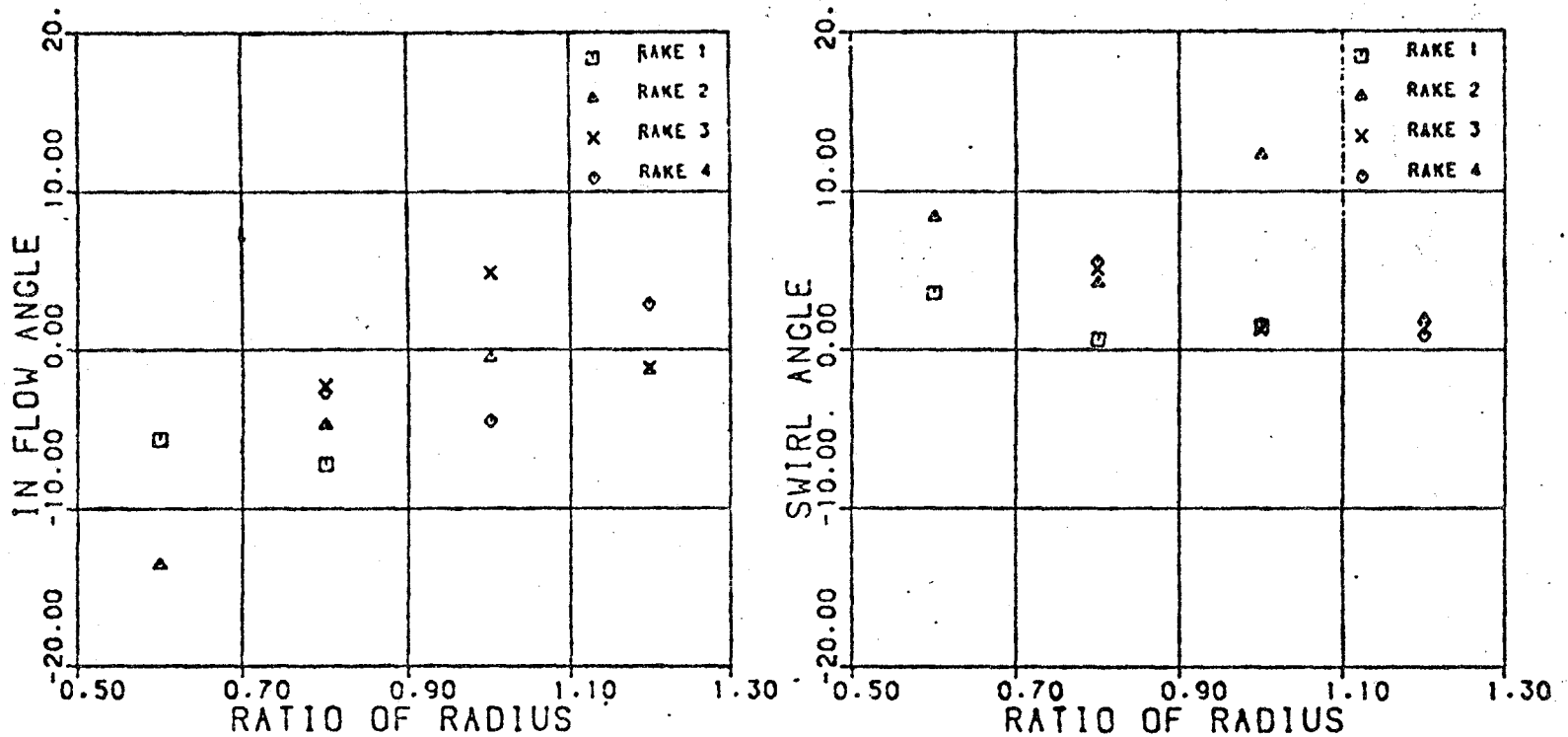

Figure 33 In-Flow and Swirl Angle for Test Run 247 (FW).
Engine rpm 2496, Tunnel Speed 95.4 Kmh.

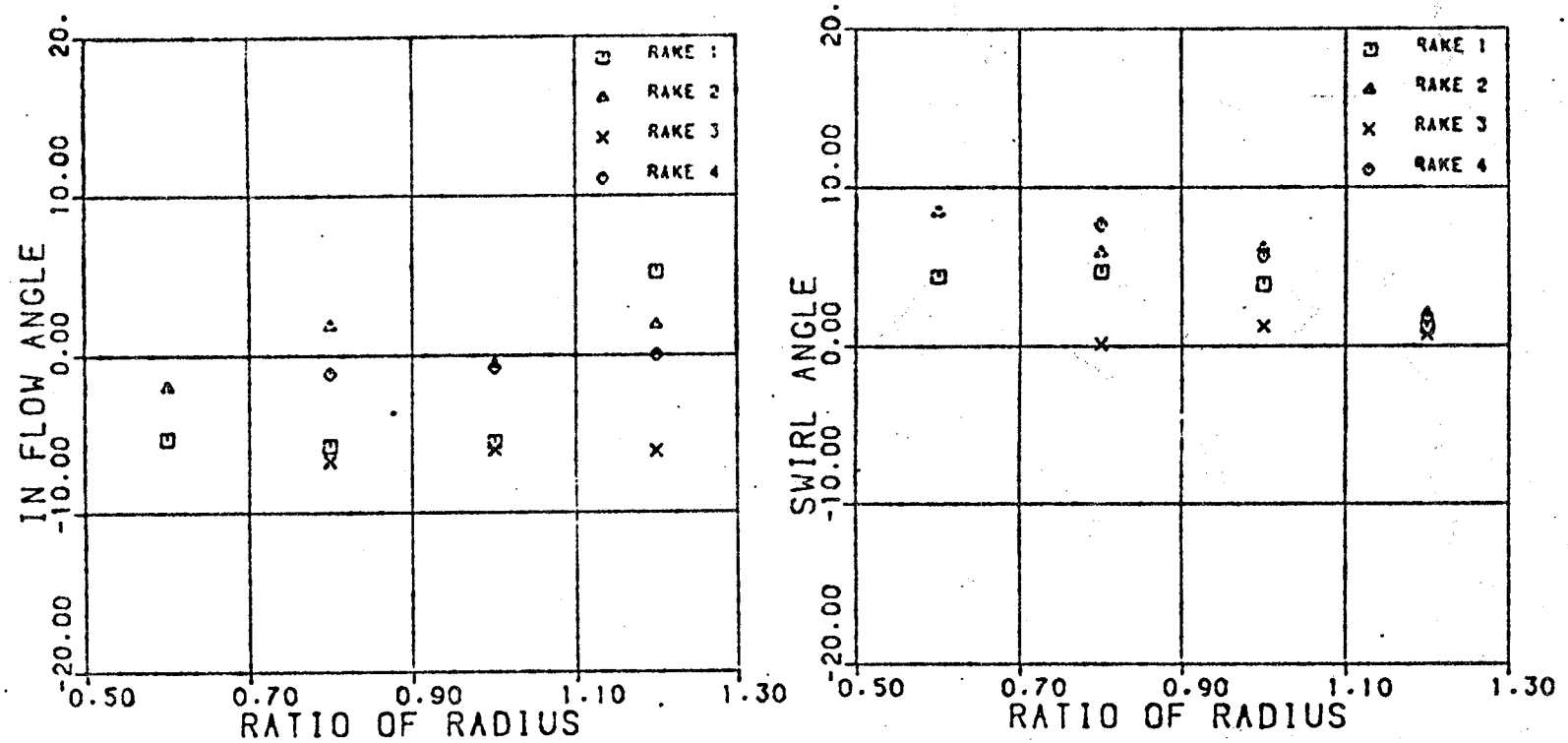

Figure 34 In-Flow and Swirl Angle for Test Run 74 (AF),
Engine rpm 1776, Tunnel Speed 95.4 Kmh.

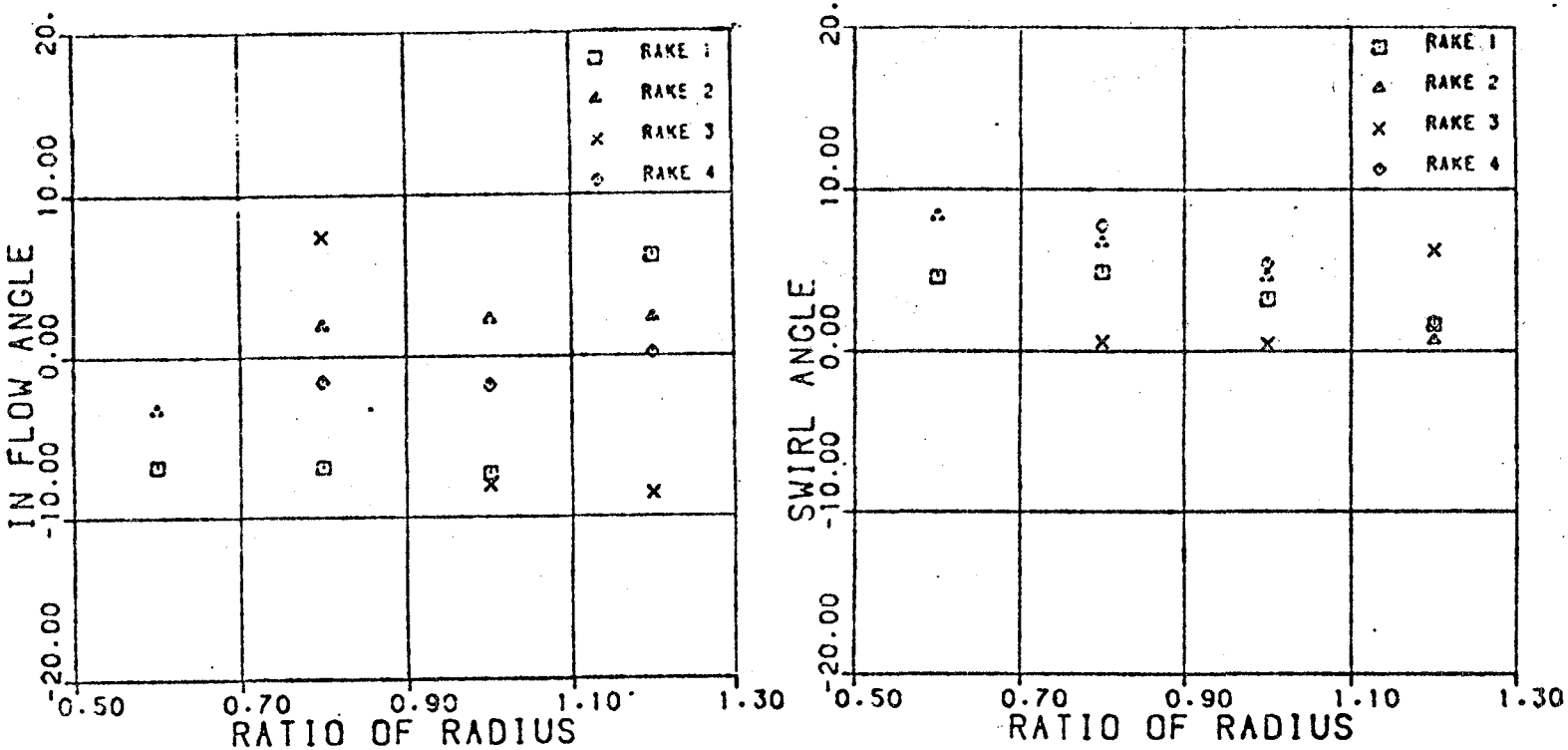

Figure 35 In-Flow and Swirl Angle for Test Run 36 (AF),
Engine rpm 1181, Tunnel Speed 50.0 Kmh.

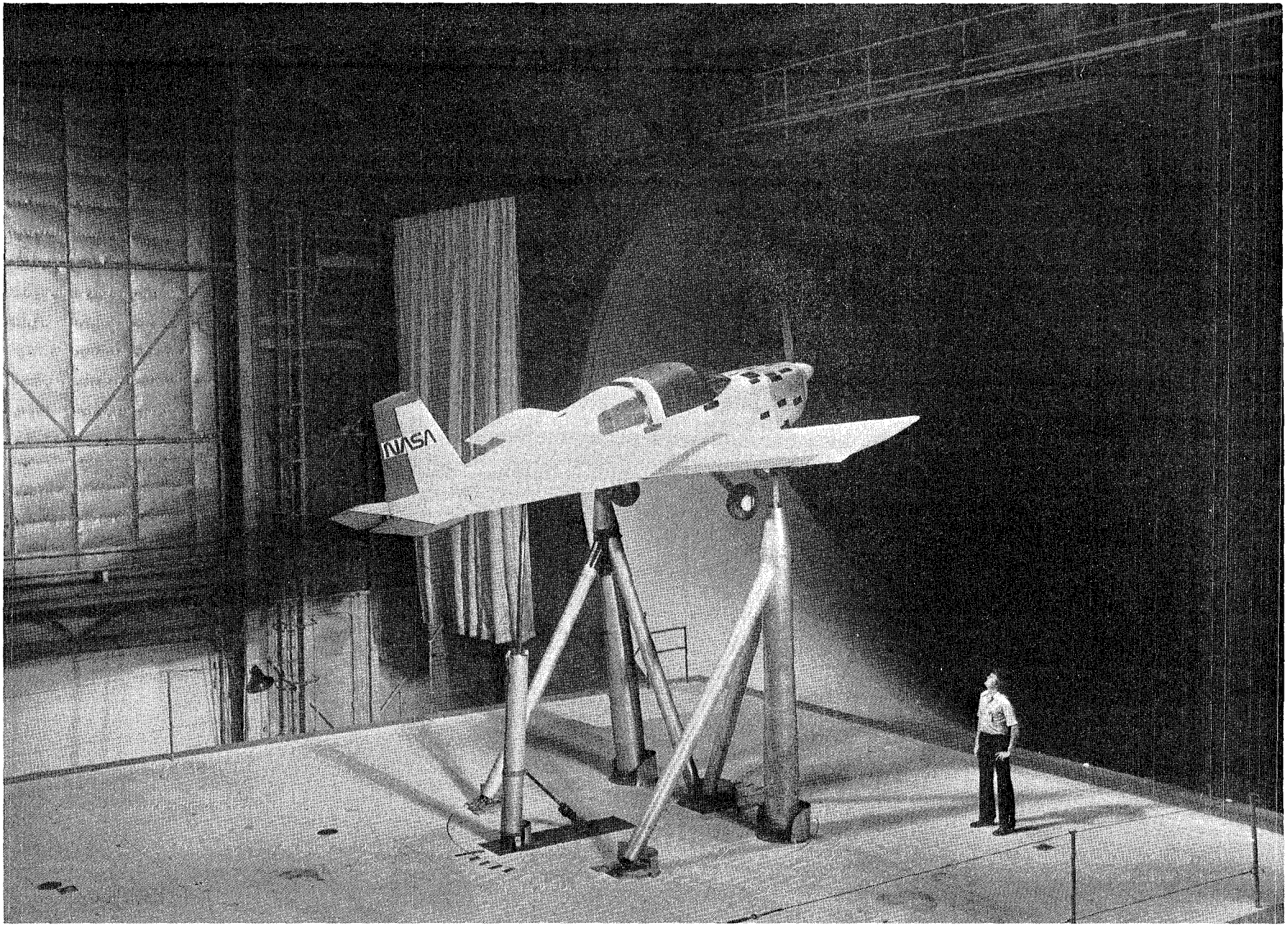

Figure 36

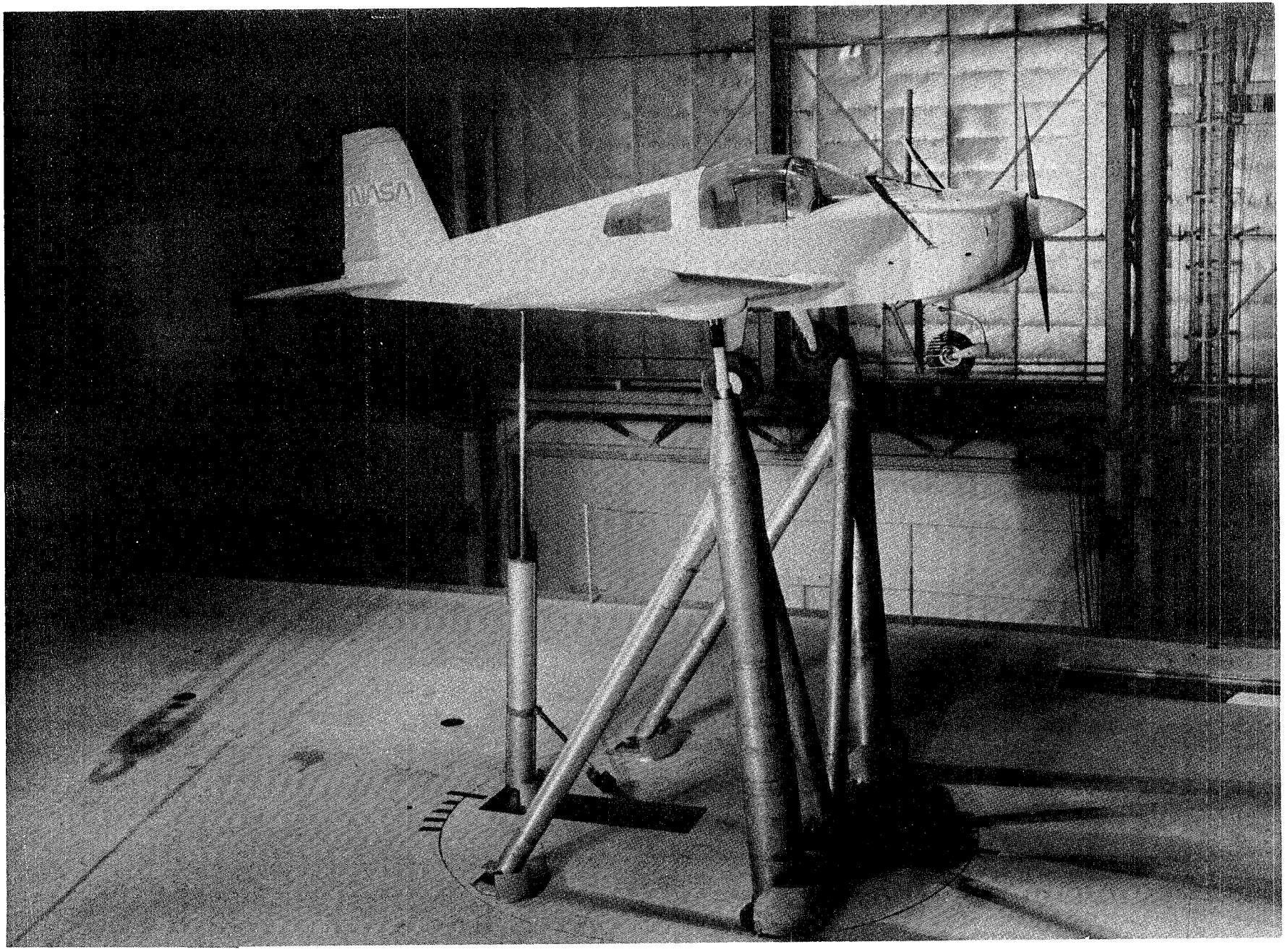

Figure 37

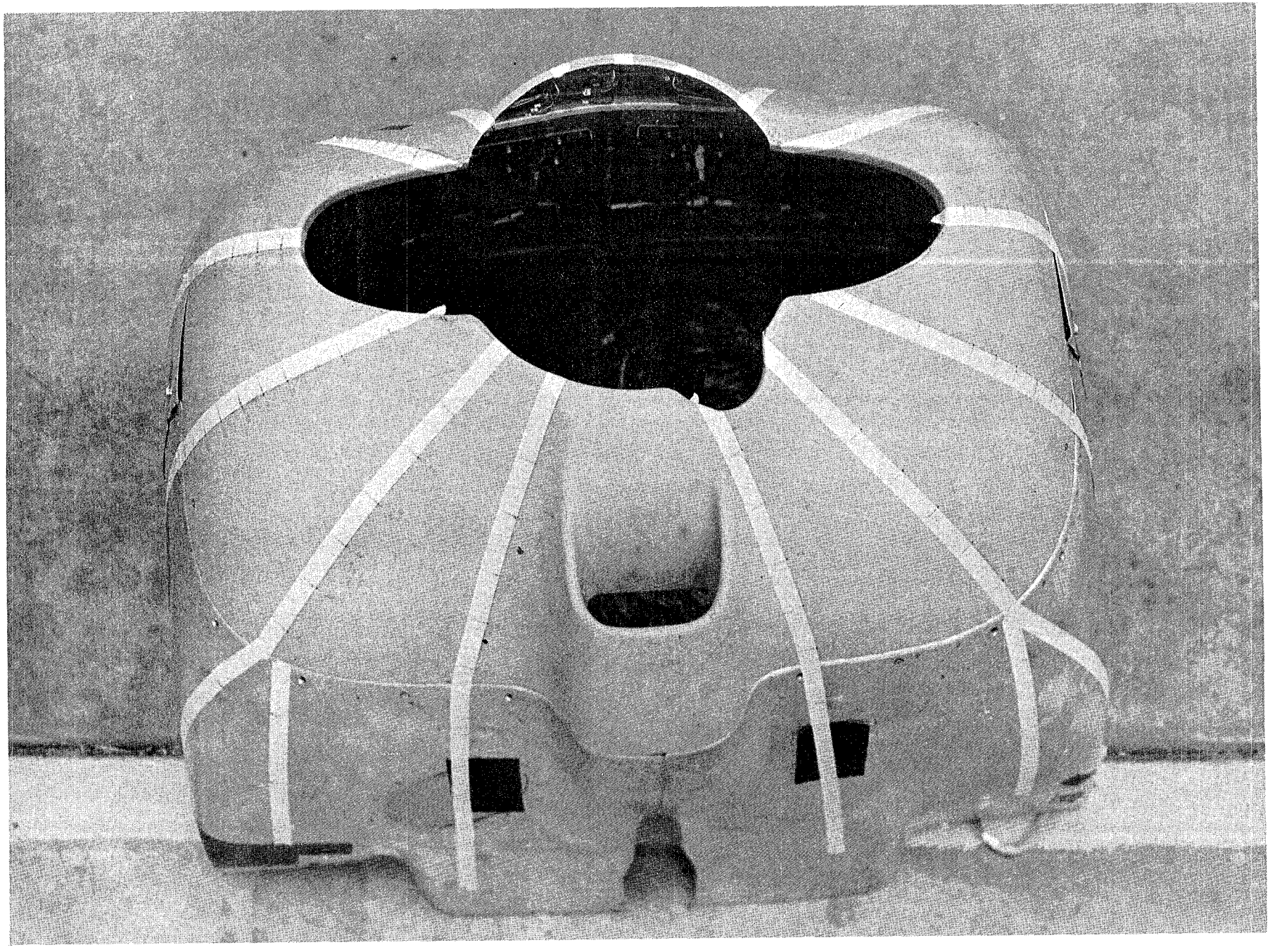

Figure 38

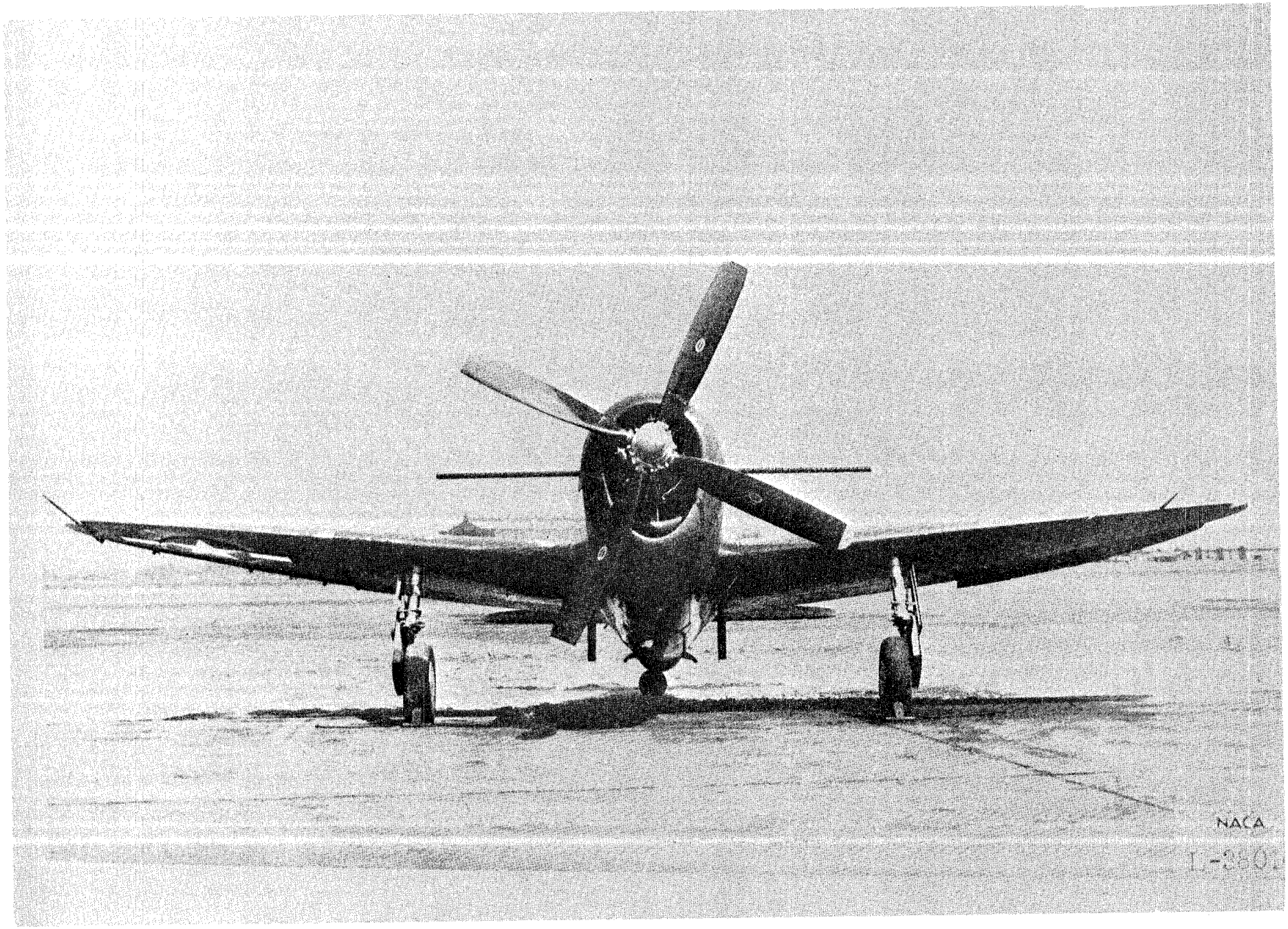

Figure 39

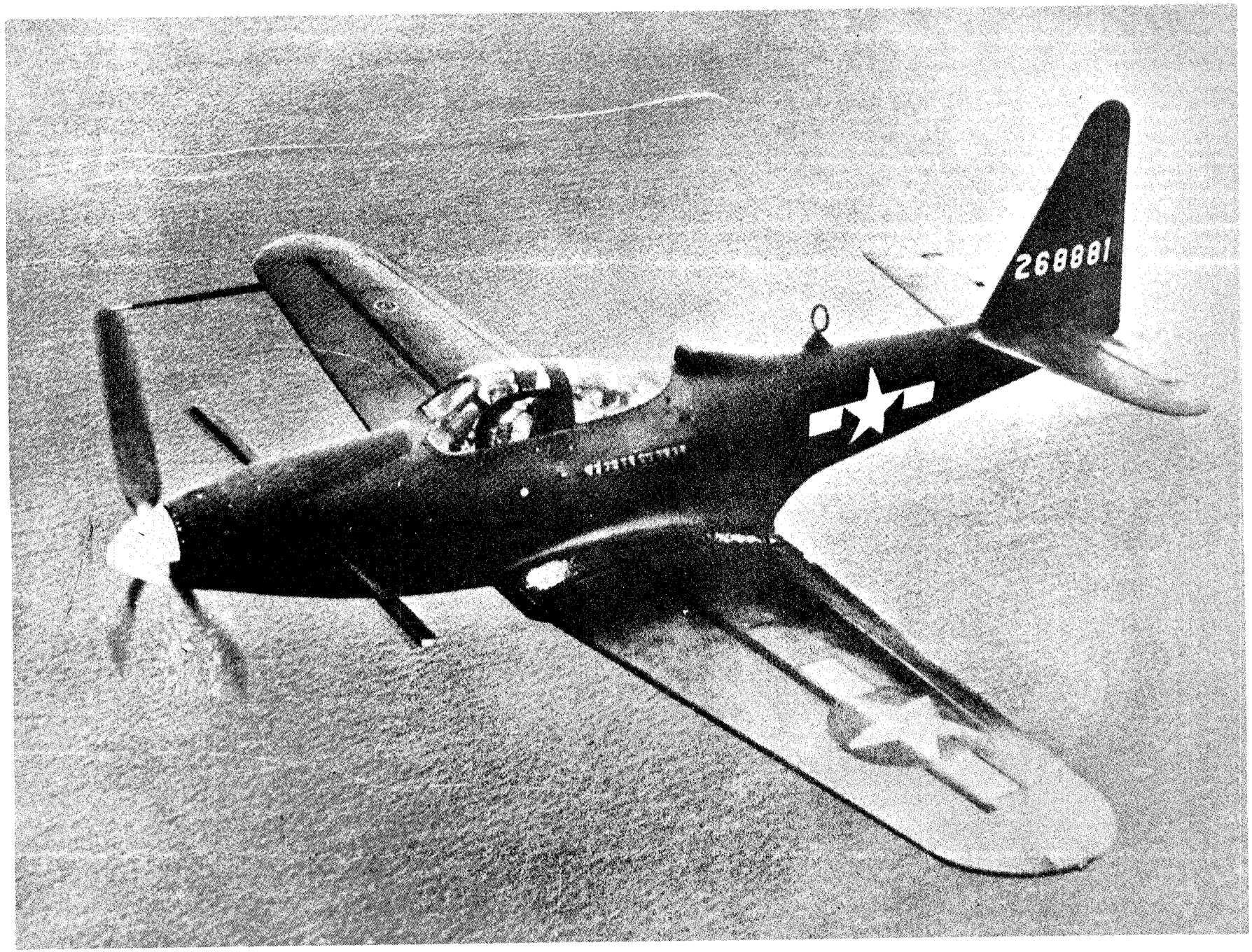

Figure 40

End of Document